Eur. Phys. J. C 1, 301–320 (1998)

THE EUROPEAN PHYSICAL JOURNAL C
© Springer-Verlag 1998

Charm electroproduction viewed in the variable-flavour number scheme versus fixed-order perturbation theory

M. Buza[1,a], Y. Matiounine[2], J. Smith[3,b], W.L. van Neerven[4]

[1] NIKHEF/UVA, POB 41882, NL-1009 DB Amsterdam, The Netherlands
[2] Institute for Theoretical Physics, State University of New York at Stony Brook, New York 11794-3840, USA
[3] Deutsches Electronen-Synchrotron DESY Notkestrasse 85, D-22603, Hamburg, Germany
[4] Instituut-Lorentz, University of Leiden, PO Box 9506, NL-2300 RA Leiden, The Netherlands

Received: 9 April 1997

Abstract. Starting from fixed-order perturbation theory (FOPT) we derive expressions for the heavy-flavour components of the deep-inelastic structure functions ($F_{i,H}(x,Q^2,m_H^2), i=2,L; H=c,b,t$) in the variable-flavour number scheme (VFNS). These expressions are valid in all orders of perturbation theory. This derivation establishes a relation between the parton densities parametrized at n_f and n_f+1 light flavours. One of the results is that the heavy quark parton density does not vanish when the factorization scale becomes equal to m_H contrary to what is assumed in the literature. Further we observe that in charm electroproduction the exact and asymptotic expressions for the heavy-quark coefficient functions yield identical results for $F_{2,c}(x,Q^2,m_c^2)$ when $x<0.01$ and $Q^2>20$ $(\mathrm{GeV}/c)^2$. From this observation and an analysis of the size of the higher order corrections we conclude that in this region the VFNS description of $F_{2,c}$ is better than the one given by FOPT. On the other hand in the charm threshold region i.e. $x>0.01$ and $Q^2<20$ $(\mathrm{GeV}/c)^2$ it turns out that the reverse is true.

1 Introduction

The study of charm production in deep-inelastic electron-proton scattering and in photon-proton scattering provides us with important information about heavy-quark-production mechanisms. Here we can distinguish between intrinsic- [1] and extrinsic-charm [2] production. In the former case the charm quark appears in the initial state and it is considered to be a part of the hadronic wave function so that the dominant production mechanism is given by the flavour excitation process. Hence this quark is described by a parton density in the hadron, as in the cases of the other light flavours (u,d,s) and the gluon (g). When the charm quark is produced extrinsically it only appears in the final state and the dominant subprocess is given by (virtual) photon-gluon-fusion, which is the only reaction present on the Born level [2]. Hence one can measure the x-dependence of the gluon density $G(x,\mu^2)$, where x denotes the Bjorken scaling variable and μ stands for the factorization and renormalization scales. Next-to-leading (NLO) corrections [3,4], to which also other processes contribute, reveal that this picture remains unaltered. From the photon-gluon-fusion subprocess one also infers that both the charm quark and the charm anti-quark appear back-to-back in the final state. This is not the case for intrinsic charm production because of the dominance of the flavour excitation process. Recent experiments carried out at HERA at $Q^2=0$ [5] (photoproduction) or at $10<Q^2<100$ $(\mathrm{GeV}/c)^2$ [6] (electroproduction), where Q^2 denotes the virtual photon mass squared, give strong evidence for extrinsic-charm production. Therefore we only concentrate on the latter production mechanism in this paper.

As has been mentioned above the extrinsic-charm mechanism can be studied in photoproduction ($Q^2=0$) and in electroproduction ($Q^2>0$). The photoproduction reaction has the advantage that the production rate is much larger than in the case of electroproduction because the latter rate is suppressed by the photon propagator, which decreases when Q^2 gets larger. In the context of perturbative QCD, however, the description of electroproduction is easier due to the absence of the hadronic (resolved) photon component which contributes in photoproduction (for a discussion see [7]). Moreover electroproduction enables us to study the charm contribution to the deep-inelastic structure functions $F_2(x,Q^2)$ and $F_L(x,Q^2)$.

For the treatment of the charm component of the structure functions $F_{i,c}(x,Q^2,m_c^2)$ $(i=2,L)$ one has adopted two different prescriptions for extrinsic-charm production in the literature. The first one is advocated in [8] where the charm quark is treated as a heavy quark and its contribution is given by fixed-order perturbation theory (FOPT).

[a] supported by the Foundation for Fundamental Research on Matter (FOM)
[b] on leave from ITP, SUNY at Stony Brook, New York 11794-3840, USA

This involves the computation of the photon-gluon-fusion process mentioned above and its higher order corrections. Hence the structure functions $F_{i,c}$ are expressed into convolutions of heavy quark coefficient functions with the three light-flavour densities (u,d,s) and the gluon density (three-flavour scheme). The second approach is to describe charm production by introducing a charm quark density which we will denote by $f_c(x,\mu^2)$. This procedure is very often refered as the variable flavour number scheme (VFNS) although its meaning is somehow different (see [9]). In this scheme the structure functions $F_{i,c}$ are presented as convolutions of light-parton coefficient functions with four light-flavour densities (u,d,s,c) and the gluon density (four-flavour scheme). At first sight this looks similar to intrinsic-charm production. However in the case of VFNS the x-dependence of the charm quark density is determined via the renormalization group equations (RGE) by the three light-flavour densities and the gluon density where one very often imposes the boundary condition $f_c(x,m_c^2)=0$. These properties do not exist in the intrinsic charm approach where this density is obtained from a model.

It is clear that the VFNS-procedure is not very well suited to describe charm production in the threshold region because the photon-gluon fusion process requires that the charm component of the structure function vanishes for $s = Q^2(1-x)/x < 4m_c^2$. This threshold condition does not show up in the x-behaviour of $f_c(x,\mu^2)$. On the other hand FOPT also has its drawbacks when Q^2 gets very large. The reason is that the heavy-quark coefficient functions calculated up to NLO in [4] are dominated by large logarithms of the type $\ln^i(Q^2/m_c^2)\ln^j(\mu^2/m_c^2)$ when $Q^2 \gg m_c^2$ [10]. Although it was shown in NLO [11] that these logarithms lead to rather stable charm structure functions $F_{i,c}(x,Q^2,m_c^2)$ with respect to variations in the factorization and renormalization scales μ, their size still warrants some special treatment (for a discussion of the scale dependence of the charm contribution in the FOPT and VFNS approaches see also [12–14]). However as we will show in this paper the above criterion is not sufficient to decide about the rate of convergence of the perturbation series. It still may happen that these large logarithms vitiate the perturbation series, in particular when corrections beyond NLO are included. Hence these logarithms have to be resummed using the standard techniques of the renormalization group.

Various attempts have been made in the literature to give a description of $F_{i,c}$ between the regions near and far above threshold. They are known by what we will call the true VFNS. Examples are given in [9] and recently also in [15]. Here the number of light flavours changes by one unit while going from the threshold domain to the asymptotic region. The goal of our paper will be different. In Sect. 2 we want to show that there exists a direct relation between FOPT at large Q^2 and the charm quark density approach which is usually called VFNS. This relation follows from the property of mass factorization shown by the large logarithmic terms $\ln^i(Q^2/m_c^2)\ln^j(\mu^2/m_c^2)$ present in the asymptotic heavy quark coefficient functions. Therefore in the large Q^2-limit one can write the asymptotic FOPT structure functions $F_{i,c}$ as convolutions of the light parton coefficient functions with the four light flavour densities (u,d,s,c) and the gluon density characteristic of VFNS. In this way one establishes relations between the parton densities in the three and four flavour schemes. In particular it turns out that one can express the charm quark density $f_c^{\rm VFNS}(x,\mu^2)$ into the parton densities present in the three light flavour scheme (FOPT). The most important outcome of this expression is that $f_c^{\rm VFNS}(x,m_c^2)\neq 0$ in the $\overline{\rm MS}$-scheme contrary to what is imposed on the charm quark density in the literature. The difference between our expression for $F_{i,c}^{\rm VFNS}$ and the one in (9) of [9] is stressed. A generalization of $F_{i,c}^{\rm VFNS}$ as presented in (9) of [9] will be given in all orders of perturbation theory. In Sect. 3 we investigate at which Q^2 the large logarithms in the heavy-quark coefficient functions actually dominate the charm component of the structure functions. We will also study the differences between the FOPT approach and the VFNS approach for the charm component of the deep-inelastic structure functions in the x- and Q^2-range explored by present experiments. Finally we investigate which approach is more stable with respect to higher order corrections to the charm structure functions. The heavy quark operator matrix elements (OME's) needed for the mass factorization of the asymptotic part of the heavy quark coefficient functions, which are represented by the large logarithms above, are presented in Appendices A and B. In Appendix A we present some heavy-quark OME's which were not previously calculated in the literature. In Appendix B we list all renormalized heavy-quark OME's which are needed for our analysis in Sect. 3.

2 Derivation of the VFNS representation of the structure functions

In this section we present the variable-flavour number scheme (VFNS) representation of the structure functions $F_i(x,Q^2)$ in all orders of perturbation theory. Our results hold for any species of heavy quark although at present collider energies the VFNS is only interesting for the charm quark. As mentioned in the previous section logarithms of the type $\ln^i(Q^2/m^2)\ln^j(\mu^2/m^2)$ arise in the heavy-quark coefficient functions when $Q^2 \gg m^2$ and we work in fixed-order perturbation theory (FOPT). Here m stands for the mass of the heavy quark, denoted by H in the subsequent part of this section. When going from the FOPT representation for the structure functions to that of the VFNS one has to remove these mass-singular logarithms from the heavy-quark coefficient functions. This is achieved using the technique of mass factorization, which is a generalization to all orders in perturbation theory of the procedure carried out up to lowest order (LO) in Sects. II D and II E in [9]. Although this procedure resembles the usual mass factorization of the collinear singularities, which appear in the partonic structure functions or partonic cross sections, it is actually much more complicated. This is due to the presence of the light (u,d,s and g) par-

tons, as well as of the heavy (c,b and t) quarks, in the Feynman diagrams describing heavy-flavour production.

In the calculations of the heavy-flavour cross sections the light partons are usually taken to be massless, whereas the heavy quarks get a mass $m \neq 0$. Note that the mass is defined by on-mass-shell renormalization. When $Q^2 \gg m^2$ two types of collinear singularities appear in the partonic contributions. One type can be attributed to the light partons. In this case the collinear divergences can be regularized using various techniques. The most well-known among them is n-dimensional regularization. The second type can be traced back to the heavy quark and the singularity manifests itself as $m \to 0$ in the large logarithmic terms mentioned above. Beyond order α_s both types of singularities appear in the partonic cross sections and in the heavy-quark operator matrix elements (OME's). The latter show up in the mass-factorization formulae, and they are needed to remove the mass-singular terms (as $m \to 0$) from the heavy-quark coefficient functions. Hence the mass factorization becomes much more complicated than when we only have to deal with collinear divergences due to massless partons. Therefore we first present the mass factorization with respect to the latter before we apply this technique to the mass singularities related to the heavy-quark mass m.

Consider first deep-inelastic electron-proton scattering in which only light-partons show up in the calculation of the QCD corrections. The deep-inelastic structure function $F_i(n_f, Q^2)$ can be expressed as follows

$$F_i(n_f,Q^2) = \frac{1}{n_f}\sum_{k=1}^{n_f} e_k^2 \Bigg[\hat{\Sigma}(n_f) \otimes \hat{\mathcal{F}}_{i,q}^{\rm S}\Big(n_f, \frac{Q^2}{p^2}, \mu^2\Big) + \hat{G}(n_f) \otimes \hat{\mathcal{F}}_{i,g}^{\rm S}\Big(n_f, \frac{Q^2}{p^2}, \mu^2\Big) + n_f \hat{\Delta}_k(n_f) \otimes \hat{\mathcal{F}}_{i,q}^{\rm NS}\Big(n_f, \frac{Q^2}{p^2}, \mu^2\Big)\Bigg] . \quad (2.1)$$

In this equation the charge of the light quark is represented by e_k and n_f denotes the number of light flavours. Further $\otimes$ denotes the convolution symbol and, for convenience, the dependence of all the above quantities on the hadronic scaling variable x and the partonic scaling variable z is suppressed. The bare quantities in (2.1) are indicated by a hat in order to distinguish them from their finite analogues, which emerge after mass factorization. Starting with the parton densities, $\hat{\Sigma}(n_f)$ and $\hat{G}(n_f)$ denote the singlet combination of light-quark densities and the gluon density respectively, with n_f light flavours. The former is given by

$$\hat{\Sigma}(n_f) = \sum_{l=1}^{n_f} \Big[\hat{f}_l(n_f) + \hat{f}_{\bar{l}}(n_f) \Big] , \quad (2.2)$$

where $\hat{f}_l(n_f)$ and $\hat{f}_{\bar{l}}(n_f)$ stand for the light-quark and light-anti-quark densities respectively. The non-singlet combination of light-quark densities is given by

$$\hat{\Delta}_k(n_f) = \hat{f}_k(n_f) + \hat{f}_{\bar{k}}(n_f) - \frac{1}{n_f}\hat{\Sigma}(n_f) . \quad (2.3)$$

The QCD radiative corrections due to the (virtual) photon light-parton subprocesses are described by the partonic structure functions $\hat{\mathcal{F}}_{i,l}(n_f)$ $(i = 2, L; l = q, g)$ where l stands for the parton which appears in the initial state. As with the parton densities they can also be classified into singlet, non-singlet and gluonic parts. Furthermore we assume that coupling-constant renormalization has been performed on the partonic (bare) structure functions, which is indicated by their dependence on the renormalization scale μ. However they still contain collinear divergences which, for convenience, are regularized by taking the external momentum p of the incoming parton off-mass-shell ($p^2 < 0$). Notice that these divergences do not show up in the final state because the deep-inelastic structure functions are totally-inclusive quantities.

The reason we choose off-shell regularization is that it allows us to distinguish between the collinear divergences coming from the massless partons and from the heavy quarks. The former divergences are the $\ln^i(-\mu^2/p^2)$ terms in the perturbative expansion, whereas the latter are the $\ln^i(\mu^2/m^2)$ terms.

We can now also reexpress (2.1) in finite quantities so that the collinear divergences are absent. This is achieved via mass factorization which proceeds as follows

$$\hat{\mathcal{F}}_{i,q}^{\rm NS}\Big(n_f, \frac{Q^2}{p^2}, \mu^2\Big) = A_{qq}^{\rm NS}\Big(n_f, \frac{\mu^2}{p^2}\Big) \otimes \mathcal{C}_{i,q}^{\rm NS}\Big(n_f, \frac{Q^2}{\mu^2}\Big) , \quad (2.4)$$

and

$$\hat{\mathcal{F}}_{i,k}^{\rm S}\Big(n_f, \frac{Q^2}{p^2}, \mu^2\Big) = \sum_{l=q,g} A_{lk}^{\rm S}\Big(n_f, \frac{\mu^2}{p^2}\Big) \otimes \mathcal{C}_{i,l}^{\rm S}\Big(n_f, \frac{Q^2}{\mu^2}\Big) . \quad (2.5)$$

In the above expressions $\mathcal{C}_{i,k} (i = 2, L; k = q, g)$ denote the light-parton coefficient functions and the A_{lk} represent the renormalized operator-matrix elements (OME's) which are defined by

$$A_{lk}\Big(n_f, \frac{\mu^2}{p^2}\Big) = < k(p)|O_l(0)|k(p) > , \quad (l, k = q, g) . \quad (2.6)$$

Here O_l are the renormalized operators which appear in the operator-product expansion of two electromagnetic currents near the light cone. The product of these two currents is sandwiched between proton states and its Fourier transform into momentum space defines the structure functions in (2.1). Like the other quantities $\mathcal{C}_{i,k}$ and A_{lk} can be divided into singlet and non-singlet parts. The scale μ appearing in (2.4)–(2.6) originates from operator renormalization as well as from coupling-constant renormalization. Notice that the operator-renormalization scale is identical to the mass-factorization scale. Using the mass-factorization relations in (2.4), (2.5) we can cast the hadronic structure functions $F_i(n_f, Q^2)$ (2.1) into the form

$$F_i(n_f,Q^2) = \frac{1}{n_f}\sum_{k=1}^{n_f} e_k^2 \Bigg[\Sigma(n_f, \mu^2) \otimes \mathcal{C}_{i,q}^{\rm S}\Big(n_f, \frac{Q^2}{\mu^2}\Big) + G(n_f, \mu^2) \otimes \mathcal{C}_{i,g}^{\rm S}\Big(n_f, \frac{Q^2}{\mu^2}\Big)$$

$$+n_f \Delta_k(n_f,\mu^2) \otimes \mathcal{C}^{\rm NS}_{i,q}\Big(n_f, \frac{Q^2}{\mu^2}\Big)\Bigg], \quad (2.7)$$

where the finite (renormalized) parton densities Σ, Δ and G are expressed in the bare ones $\hat{\Sigma}$, $\hat{\Delta}$ and $\hat{G}$ in the following way

$$\Delta_k(n_f,\mu^2) = A^{\rm NS}_{qq}\Big(n_f, \frac{\mu^2}{p^2}\Big) \otimes \hat{\Delta}_k(n_f)\,, \quad (2.8)$$

$$\Sigma(n_f,\mu^2) = A^{\rm S}_{qq}\Big(n_f, \frac{\mu^2}{p^2}\Big) \otimes \hat{\Sigma}(n_f) + A^{\rm S}_{qg}\Big(n_f, \frac{\mu^2}{p^2}\Big) \otimes \hat{G}(n_f)\,, \quad (2.9)$$

and

$$G(n_f,\mu^2) = A^{\rm S}_{gq}\Big(n_f, \frac{\mu^2}{p^2}\Big) \otimes \hat{\Sigma}(n_f) + A^{\rm S}_{gg}\Big(n_f, \frac{\mu^2}{p^2}\Big) \otimes \hat{G}(n_f)\,. \quad (2.10)$$

All quantities given above satisfy renormalization group equations (RGE's). Here we are only interested in those RGE's for the OME's and the parton densities. Define the differential operator D as

$$D = \mu\frac{\partial}{\partial\mu} + \beta(n_f,g)\frac{\partial}{\partial g}\,, \qquad g \equiv g(n_f,\mu^2)\,, \quad (2.11)$$

where $\alpha_s = g^2/(4\pi)$, then the OME's satisfy the following RGE's

$$DA^{\rm NS}_{qq}\Big(n_f, \frac{\mu^2}{p^2}\Big) = -\gamma^{\rm NS}_{qq}(n_f) \otimes A^{\rm NS}_{qq}\Big(n_f, \frac{\mu^2}{p^2}\Big)\,, \quad (2.12)$$

$$DA^{\rm S}_{ij}\Big(n_f, \frac{\mu^2}{p^2}\Big) = -\sum_{k=q,g} \gamma^{\rm S}_{ik}(n_f) \otimes A^{\rm S}_{kj}\Big(n_f, \frac{\mu^2}{p^2}\Big)\,. \quad (2.13)$$

Here γ_{ij} denote the anomalous dimensions corresponding to the operators O_i. They can be expanded as a perturbation series in α_s. In Bjorken x-space there exists a relation between the anomalous dimensions γ_{ij} and the DGLAP splitting functions, denoted by P_{ij}, which is given by

$$\gamma_{ij}(n_f) = -P_{ij}(n_f)\,. \quad (2.14)$$

Notice that this relation only holds for twist-two operators. From the above equation one infers that the γ_{ij}, which are the residues of the ultraviolet divergences in the unrenormalized OME's, have just the opposite signs to those of the P_{ij}. The latter show up in the partonic quantities $\hat{\mathcal{F}}_{i,l}(n_f)$ in (2.1) and they represent the residues of the collinear divergences. We will return to this relation (2.14) when we discuss the heavy-quark OME's. The finite (renormalized) parton densities satisfy the RGE's

$$D\Delta_k(n_f,\mu^2) = -\gamma^{\rm NS}_{qq}(n_f) \otimes \Delta_k(n_f,\mu^2)\,, \quad (2.15)$$

$$D\Sigma(n_f,\mu^2) = -\gamma^{\rm S}_{qq}(n_f) \otimes \Sigma(n_f,\mu^2) - \gamma^{\rm S}_{qg}(n_f) \otimes G(n_f,\mu^2)\,, \quad (2.16)$$

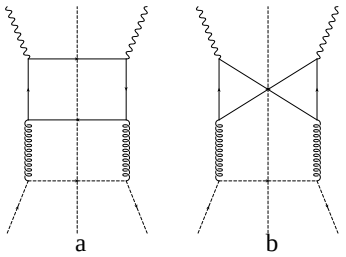

Fig. 1. $O(\alpha_s^2)$ contributions to the purely-singlet parton structure function $\mathcal{F}^{\rm PS}_{i,q}$ representing the subprocess $\gamma^* + q \to q + q' + \bar{q}'$. Here q and q' are represented by the *dashed* and *solid lines* respectively. In the case of heavy-quark production $q' = H$ and these graphs contribute to the heavy-quark coefficient function $H^{\rm PS}_{i,q}$

and

$$DG(n_f,\mu^2) = -\gamma^{\rm S}_{gq}(n_f) \otimes \Sigma(n_f,\mu^2) - \gamma^{\rm S}_{gg}(n_f) \otimes G(n_f,\mu^2)\,. \quad (2.17)$$

From these equations we can derive the Altarelli-Parisi equations.

Before we add the heavy-quark contributions to the deep-inelastic structure functions (2.7) it is convenient to split the singlet quantities $\hat{\mathcal{F}}^{\rm S}_{i,q}$, $\mathcal{C}^{\rm S}_{i,q}$ and $A^{\rm S}_{qq}$ into non-singlet and purely-singlet parts, namely

$$\hat{\mathcal{F}}^{\rm S}_{i,q} = \hat{\mathcal{F}}^{\rm NS}_{i,q} + \hat{\mathcal{F}}^{\rm PS}_{i,q}\,, \quad (2.18)$$

$$\mathcal{C}^{\rm S}_{i,q} = \mathcal{C}^{\rm NS}_{i,q} + \mathcal{C}^{\rm PS}_{i,q}\,, \quad (2.19)$$

and

$$A^{\rm S}_{qq} = A^{\rm NS}_{qq} + A^{\rm PS}_{qq}\,. \quad (2.20)$$

This decomposition facilitates the mass factorization of the heavy-quark coefficient functions and can be explained as follows. If we calculate the diagrams contributing to the parton subprocesses with a quark in the initial state, the resulting expressions have to be projected on the singlet and non-singlet channels with respect to the flavour group. The latter projection leads to $\hat{\mathcal{F}}^{\rm NS}_{i,q}$. However the singlet part i.e. $\hat{\mathcal{F}}^{\rm S}_{i,q}$ can be split into two types of contributions. The first one is equal to $\hat{\mathcal{F}}^{\rm NS}_{i,q}$ whereas the second one is represented by $\hat{\mathcal{F}}^{\rm PS}_{i,q}$. The purely-singlet partonic structure function arises from the Feynman graphs where the projection on the non-singlet channel yields zero, so that only singlet contributions remain. They are characterized by those Feynman graphs in which only gluons are exchanged in the t-channel. Such graphs show up for the first time in two-loop order. An example is given in Fig. 1. The same characteristics also hold for $A^{\rm PS}_{qq}$ (see Fig. 2) and the resulting coefficient function $\mathcal{C}^{\rm PS}_{i,q}$. Another important feature is that the purely-singlet quantities are proportional to the number of light flavours n_f. This property is shared by the gluonic quantities $\hat{\mathcal{F}}^{\rm S}_{i,g}$, $\mathcal{C}^{\rm S}_{i,g}$ and $A^{\rm S}_{qg}$. The proportionality to n_f can be traced back to the fact that in the case of $\hat{\mathcal{F}}^{\rm PS}_{i,q}$, $\hat{\mathcal{F}}^{\rm S}_{i,g}$ the virtual photon is attached to

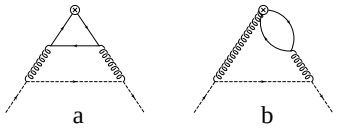

Fig. 2. $O(\alpha_s^2)$ contributions to the purely-singlet OME $A_{q'q}^{\rm PS}$. Here q and q' are represented by the *dashed* and *solid lines* respectively. In the case of $q' = H$ these graphs contribute to the heavy-quark OME $A_{Hq}^{\rm PS}$

the light-quark loop (see e.g. Fig. 1) and one has to sum over all light flavours. In the case of $A_{qq}^{\rm PS}$ and $A_{qg}^{\rm S}$ this is due to the insertion of the operator vertex into the light-quark loop where also a sum over all light flavours has to be carried out. Because of the mass-factorization relation (2.5) the proportionality to n_f is transferred to the coefficient functions $\mathcal{C}_{i,q}^{\rm PS}$, $\mathcal{C}_{i,g}^{\rm S}$ and the anomalous dimensions $\gamma_{qq}^{\rm PS}$, $\gamma_{qg}^{\rm S}$. To facilitate the mass factorization of the heavy-quark coefficient functions it is very convenient to extract this overall factor of n_f from the quantities above so we define

$$T_{i,k} = n_f \tilde{T}_{i,k}\,, \tag{2.21}$$

where

$$T_{i,q} = \hat{\mathcal{F}}_{i,q}^{\rm PS}, \mathcal{C}_{i,q}^{\rm PS}\,; \qquad T_{i,g} = \hat{\mathcal{F}}_{i,g}^{\rm S}, \mathcal{C}_{i,g}^{\rm S}\,; \tag{2.22}$$

and

$$R_{ij} = n_f \tilde{R}_{ij}\,, \tag{2.23}$$

where

$$R_{qq} = A_{qq}^{\rm PS}, \gamma_{qq}^{\rm PS}\,; \qquad R_{qg} = A_{qg}^{\rm S}\,, \gamma_{qg}^{\rm S}\,. \tag{2.24}$$

Besides the overall dependence on n_f, which we have extracted from the quantities defined by $T_{i,k}$ and R_{ij} above, there still remains a residual dependence on n_f in $\tilde{T}_{i,k}$ and $\tilde{R}_{ij}$. The latter dependence originates from internal light-flavour loops which are neither attached to the virtual photon nor to the operator-vertex insertions. Since there are more contributions to $\tilde{T}_{i,k}$ and $\tilde{R}_{ij}$ which are not due to these light flavour-loops it is impossible to extract an overall factor n_f anymore from the quantities indicated by a tilde. Therefore the dependence of the latter on n_f means that it can be only attributed to internal light-flavour loops. Using the above definitions one can now rewrite (2.1) and (2.7) and the results become

$$\begin{aligned} F_i(n_f,Q^2) = \sum_{k=1}^{n_f} e_k^2 \Bigg[& \hat{\Sigma}(n_f) \otimes \tilde{\hat{\mathcal{F}}}_{i,q}^{\rm PS}\Big(n_f, \frac{Q^2}{p^2}, \mu^2\Big) \\ & + \hat{G}(n_f) \otimes \tilde{\hat{\mathcal{F}}}_{i,g}^{\rm S}\Big(n_f, \frac{Q^2}{p^2}, \mu^2\Big) \\ & + \Big\{ \hat{f}_k(n_f) + \hat{f}_{\bar{k}}(n_f) \Big\} \otimes \hat{\mathcal{F}}_{i,q}^{\rm NS}\Big(n_f, \frac{Q^2}{p^2}, \mu^2\Big) \Bigg]\,, \end{aligned} \tag{2.25}$$

$$\begin{aligned} F_i(n_f,Q^2) = \sum_{k=1}^{n_f} e_k^2 \Bigg[& \Sigma(n_f,\mu^2) \otimes \tilde{\mathcal{C}}_{i,q}^{\rm PS}\Big(n_f, \frac{Q^2}{\mu^2}\Big) \\ & + G(n_f,\mu^2) \otimes \tilde{\mathcal{C}}_{i,g}^{\rm S}\Big(n_f, \frac{Q^2}{\mu^2}\Big) \\ & + \Big\{ f_k(n_f,\mu^2) + f_{\bar{k}}(n_f,\mu^2) \Big\} \otimes \mathcal{C}_{i,q}^{\rm NS}\Big(n_f, \frac{Q^2}{\mu^2}\Big) \Bigg]\,, \end{aligned} \tag{2.26}$$

with the relation

$$\begin{aligned} & f_k(n_f,\mu^2) + f_{\bar{k}}(n_f,\mu^2) \\ & \quad = A_{qq}^{\rm NS}\Big(n_f, \frac{\mu^2}{p^2}\Big) \otimes \Big\{ \hat{f}_k(n_f) + \hat{f}_{\bar{k}}(n_f) \Big\} \\ & \quad + \tilde{A}_{qq}^{\rm PS}\Big(n_f, \frac{\mu^2}{p^2}\Big) \otimes \hat{\Sigma}(n_f) + \tilde{A}_{qg}^{\rm S}\Big(n_f, \frac{\mu^2}{p^2}\Big) \otimes \hat{G}(n_f)\,. \end{aligned} \tag{2.27}$$

Using (2.5), (2.9) and (2.10) one can now write the mass factorization relations for the quantities indicated by $\tilde{T}_{i,k}$ and $\tilde{R}_{ij}$ in (2.21)–(2.24). The same can be done for the RGE's which can be derived from (2.13), (2.16) and (2.17). Since this derivation is easy it is left to the reader. Here we only want to report the RGE for the left-hand-side of (2.27) which follows from (2.15) and (2.16). It is given by

$$\begin{aligned} & D[f_k(n_f,\mu^2) + f_{\bar{k}}(n_f,\mu^2)] \\ & \quad = -\gamma_{qq}^{NS}(n_f) \otimes \Big[f_k(n_f,\mu^2) + f_{\bar{k}}(n_f,\mu^2) \Big] \\ & \quad - \tilde{\gamma}_{qq}^{\rm PS}(n_f) \otimes \Sigma(n_f,\mu^2) - \tilde{\gamma}_{qg}^{\rm S}(n_f) \otimes G(n_f,\mu^2)\,. \end{aligned} \tag{2.28}$$

After having presented the formulae needed for the mass factorization of the light-parton structure functions $\hat{\mathcal{F}}_{i,l}$ with the corresponding RGE's we want to deal in a similar way with the asymptotic heavy-quark coefficient functions where the large logarithmic terms depending on the heavy-quark mass m have to be removed. For that purpose we have to add the heavy-quark contribution to the deep-inelastic structure function $F_i(n_f,Q^2)$ (2.26). The former is

$$\begin{aligned} & F_{i,H}(n_f,Q^2,m^2) \\ & \quad = \sum_{k=1}^{n_f} e_k^2 \Bigg[\Sigma(n_f,\mu^2) \otimes \tilde{L}_{i,q}^{\rm PS}\Big(n_f, \frac{Q^2}{m^2}, \frac{m^2}{\mu^2}\Big) \\ & \quad + G(n_f,\mu^2) \otimes \tilde{L}_{i,g}^{\rm S}\Big(n_f, \frac{Q^2}{m^2}, \frac{m^2}{\mu^2}\Big) \\ & \quad + \Big\{ f_k(n_f,\mu^2) + f_{\bar{k}}(n_f,\mu^2) \Big\} \otimes L_{i,q}^{\rm NS}\Big(n_f, \frac{Q^2}{m^2}, \frac{m^2}{\mu^2}\Big) \Bigg] \\ & \quad + e_H^2 \Bigg[\Sigma(n_f,\mu^2) \otimes H_{i,q}^{\rm PS}\Big(n_f, \frac{Q^2}{m^2}, \frac{m^2}{\mu^2}\Big) \\ & \quad + G(n_f,\mu^2) \otimes H_{i,g}^{\rm S}\Big(n_f, \frac{Q^2}{m^2}, \frac{m^2}{\mu^2}\Big) \Bigg]\,, \end{aligned} \tag{2.29}$$

where e_H stands for the charge of the heavy quark denoted by H. Further $L_{i,k}$ and $H_{i,k} (i = 2, L; k = q, g)$ represent the heavy-quark coefficient functions. Like in the case of

the light-parton coefficient functions $\mathcal{C}_{i,k}$ they can be split into singlet and non-singlet parts. The former can be decomposed into non-singlet and purely-singlet pieces in a similar way as given in (2.19). The distinction between $L_{i,k}$ and $H_{i,k}$ can be traced back to the different (virtual) photon-parton heavy-quark production mechanisms from which they originate. The functions $L_{i,k}$ are attributed to the reactions where the virtual photon couples to the light quarks (u, d, and s), whereas the $H_{i,k}$ describe the interactions between the virtual photon and the heavy quark. Hence $L_{i,k}$ and $H_{i,k}$ in (2.29) are multiplied by e_k^2 and e_H^2 respectively. Moreover, when the reaction where the photon couples to the heavy quark contains a light quark in the initial state, then it can only proceed via the exchange of a gluon in the t-channel (see Fig. 1). Therefore $H_{i,q}$ is purely-singlet and a non-singlet contribution does not exist. This is in contrast with $L_{i,q}$ which has both purely-singlet and non-singlet contributions. Finally we want to emphasize that all radiative corrections containing a heavy quark in the loops are included in the heavy quark coefficient functions of (2.29). Only in this case do the latter have the appropriate asymptotic Q^2-behaviour so that mass factorization with respect to m^2 is possible.

We will now study (2.29) for asymptotic Q^2-values. Therefore we define

$$F_{i,H}^{\rm asymp}(n_f, Q^2, m^2) = \lim_{Q^2 \gg m^2} \Big[F_{i,H}(n_f, Q^2, m^2) \Big] . \tag{2.30}$$

The asymptotic heavy quark structure function $F_{i,H}^{\rm asymp}$ has the same form as $F_{i,H}^{\rm exact}$ in (2.29) except that the exact heavy quark coefficient functions are replaced by the asymptotic ones denoted by $L_{i,k}^{\rm asymp}$ and $H_{i,k}^{\rm asymp} (i = 2, L; k = q, g)$. The latter are only given by the large logarithms, mentioned at the beginning of this section, including constant terms. If these terms become too large they vitiate the perturbation series so that a resummation via the RGE is necessary. Before this resummation can be carried out we have first to perform mass factorization to remove the mass-singular terms $\ln^i(\mu^2/m^2)$ from the asymptotic heavy-quark coefficient functions. This can be done in a similar way as shown for the partonic structure functions in (2.4), (2.5), where now $\ln^i(-\mu^2/p^2)$ are replaced by $\ln^i(\mu^2/m^2)$.

To perform the mass factorization one has first to add $F_{i,H}^{\rm asymp}(n_f, Q^2, m^2)$ to the structure function $F_i(n_f, Q^2)$ in (2.26). Then the mass factorization relations for the coefficient functions $L_{i,k}^{\rm asymp}$ read as follows

$$\mathcal{C}_{i,q}^{\rm NS}(n_f) + L_{i,q}^{\rm asymp,NS}(n_f) = A_{qq,H}^{\rm NS}(n_f) \otimes \mathcal{C}_{i,q}^{\rm NS}(n_f + 1), \tag{2.31}$$

$$\begin{aligned} &\tilde{\mathcal{C}}_{i,q}^{\rm PS}(n_f) + \tilde{L}_{i,q}^{\rm asymp,PS}(n_f) \\ &= \Big[A_{qq,H}^{\rm NS}(n_f) + n_f \tilde{A}_{qq,H}^{\rm PS}(n_f) + \tilde{A}_{Hq}^{\rm PS}(n_f) \Big] \otimes \tilde{\mathcal{C}}_{i,q}^{\rm PS}(n_f + 1) \\ &+ \tilde{A}_{qq,H}^{\rm PS}(n_f) \otimes \mathcal{C}_{i,q}^{\rm NS}(n_f + 1) + A_{gq,H}^{\rm S}(n_f) \otimes \tilde{\mathcal{C}}_{i,g}^{\rm S}(n_f + 1) , \end{aligned} \tag{2.32}$$

and

$$\begin{aligned} &\tilde{\mathcal{C}}_{i,g}^{\rm S}(n_f) + \tilde{L}_{i,g}^{\rm asymp,S}(n_f) \\ &= \tilde{A}_{qg,H}^{\rm S}(n_f) \otimes \mathcal{C}_{i,q}^{\rm NS}(n_f + 1) + A_{gg,H}^{\rm S}(n_f) \otimes \tilde{\mathcal{C}}_{i,g}^{\rm S}(n_f + 1) \\ &+ \Big[n_f \tilde{A}_{qg,H}^{\rm S}(n_f) + \tilde{A}_{Hg}^{\rm S}(n_f) \Big] \otimes \tilde{\mathcal{C}}_{i,q}^{\rm PS}(n_f + 1) . \end{aligned} \tag{2.33}$$

The mass factorization relations for the heavy quark coefficient functions $H_{i,k}^{\rm asymp}$ become

$$\begin{aligned} &H_{i,q}^{\rm asymp,PS}(n_f) \\ &= \tilde{A}_{Hq}^{\rm PS}(n_f) \otimes \Big[\mathcal{C}_{i,q}^{\rm NS}(n_f + 1) + \tilde{\mathcal{C}}_{i,q}^{\rm PS}(n_f + 1) \Big] \\ &+ \Big[A_{qq,H}^{\rm NS}(n_f) + n_f \tilde{A}_{qq,H}^{\rm PS}(n_f) \Big] \otimes \tilde{\mathcal{C}}_{i,q}^{\rm PS}(n_f + 1) \\ &+ A_{gq,H}^{\rm S}(n_f) \otimes \tilde{\mathcal{C}}_{i,g}^{\rm S}(n_f + 1) , \end{aligned} \tag{2.34}$$

and

$$\begin{aligned} &H_{i,g}^{\rm asymp,S}(n_f) \\ &= A_{gg,H}^{\rm S}(n_f) \otimes \tilde{\mathcal{C}}_{i,g}^{\rm S}(n_f + 1) + n_f \tilde{A}_{qg,H}^{\rm S}(n_f) \otimes \tilde{\mathcal{C}}_{i,q}^{\rm PS}(n_f + 1) \\ &+ \tilde{A}_{Hg}^{\rm S}(n_f) \otimes \Big[\mathcal{C}_{i,q}^{\rm NS}(n_f + 1) + \tilde{\mathcal{C}}_{i,q}^{\rm PS}(n_f + 1) \Big] . \end{aligned} \tag{2.35}$$

In the above equations A_{Hk} denotes the heavy-quark OME defined by

$$A_{Hk}\Big(n_f, \frac{\mu^2}{m^2}\Big) = < k(p) | O_H(0) | k(p) > , \tag{2.36}$$

which is the analogue of the light-quark OME's in (2.6). The quantities $A_{lk,H}(n_f, \mu^2/m^2)$, which also appear above, represent the heavy-quark-loop contributions to the light-quark and gluon OME's defined in (2.6).

Although there exists some similarity between the mass factorization of $\hat{\mathcal{F}}_{i,l}$ in (2.4), (2.5) and the ones given for the heavy-quark coefficient functions above we also observe a striking difference which leads to the much more complicated (2.31)–(2.35). The main difference is that the light partons appear in the initial as well as in the final state of the subprocesses contributing to $\hat{\mathcal{F}}_{i,l}$ whereas the heavy quark only shows up in the final state of the reactions leading to $L_{i,l}$,$H_{i,l}$ (2.29). This implies that there is no analogue for $\hat{\mathcal{F}}_{i,H}$ in (2.29) meaning that the coefficient functions $L_{i,H}$ and $H_{i,H}$ do not appear in the latter equation. The same holds for the bare heavy-quark density $\hat{f}_H$ which has no counter part in (2.26) and (2.27) either. Hence the mass factorization relations in (2.31)–(2.35) are much more cumbersome than those presented in (2.4), (2.5). We have explicitly checked that the above relations hold up to order α_s^2 using the asymptotic heavy-quark coefficient functions in [10] and the heavy quark OME's in Appendix B.

Yet another complication arises when we consider the OME's A_{Hk} and $A_{lk,H}$ defined above. Contrary to the light-parton OME's in (2.6) which only depend, apart from μ^2, on one mass scale p^2 the former also depend on the mass scale m^2 due to the presence of the heavy quark. Therefore the unrenormalized expressions of A_{Hk}

and $A_{lk,H}$ contain besides ultraviolet (UV) divergences two types of collinear divergences which are represented by $\ln^i(\mu^2/p^2)$ (light partons) and $\ln^i(\mu^2/m^2)$ (heavy quark) respectively. The singularity at $p^2 = 0$ shows up because external massless lines represented by $k = q, g$ in (2.36) are coupled to internal massless quanta. This phenomenon shows up for the first time in order α_s^2 see [10]. Notice that the singularities at $p^2 = 0$ also appear in the partonic quantities leading to the heavy-quark coefficient functions before they are removed by mass factorization as outlined in the beginning of this section. Therefore we also have to subtract the collinear singularities in $p^2 = 0$ from the unrenormalized OME's A_{Hk},$A_{lk,H}$ in addition to the UV divergences. This twofold subtraction leads to two different scales in the renormalized OME's in (2.31)–(2.36) which are called the operator-renormalization scale and mass-factorization scale respectively. Usually these two scales are set to be equal and they are denoted by one parameter μ^2. However the appearance of these two scales results in more complicated RGE's for the heavy-quark OME's in comparison with those presented for the light-parton OME's in (2.12), (2.13) as we will see below. In the actual calculations of A_{Hk},$A_{lk,H}$ in [10] we have put $p^2 = 0$ in (2.36) because we did the same for the partonic quantities computed in [4] leading to the heavy-quark coefficient functions $L_{i,l}$, $H_{i,l}$. Hence we had to adopt n-dimensional regularization for the UV as well as the collinear singularities in $p^2 = 0$. In this way both are represented by pole terms of the type $1/(n-4)^j$. If the latter are removed in the $\overline{\rm MS}$-scheme the OME's A_{Hk} and $A_{lk,H}$ automatically depend on one scale μ.

Another comment we want to make is that α_s appearing in the heavy-quark coefficient functions is renormalized at n_f flavours. This means that the renormalization of the coupling constant is carried out in such a way that all quarks equal to H and heavier than H decouple in the quark loops contributing to α_s. In the right-hand-side of (2.31)–(2.35) the decoupling of the heavy quark H has been undone so that here α_s depends on $n_f + 1$ flavours. This decoupling gives rise to additional logarithms of the type $\ln^i(\mu^2/m^2)$, which are cancelled by the OME's of the type $A_{kl,H}$. However explicit indication of this procedure further complicates our mass factorization relations above, which we want to avoid, so we have to bear in mind that this decoupling is implicitly understood.

If we now insert (2.31)–(2.35) into $F_i(n_f, Q^2)$ $+F_{i,H}^{\rm asymp}(n_f, Q^2, m^2)$ and rearrange some terms then we obtain our expression for $F_i^{\rm VFNS}$ which is equal to $F_i(n_f+1, Q^2)$ in (2.26). This implies that the new parton densities taken at n_f+1 light flavours can be expressed in terms of those given for n_f flavours. The original n_f light-flavour densities get modified so that for $k = 1, \ldots, n_f$

$$
\begin{aligned}
&f_k(n_f+1,\mu^2) + f_{\bar k}(n_f+1,\mu^2)\\
&\quad = A_{qq,H}^{\rm NS}\Big(n_f, \frac{\mu^2}{m^2}\Big) \otimes \Big[f_k(n_f,\mu^2) + f_{\bar k}(n_f,\mu^2)\Big]\\
&\quad +\tilde A_{qq,H}^{\rm PS}\Big(n_f, \frac{\mu^2}{m^2}\Big) \otimes \Sigma(n_f,\mu^2)\\
&\quad +\tilde A_{qg,H}^{\rm S}\Big(n_f, \frac{\mu^2}{m^2}\Big) \otimes G(n_f,\mu^2)\,, \qquad (2.37)
\end{aligned}
$$

whereas the parton density of the heavy quark can be expressed in the original light flavours in the following way

$$
\begin{aligned}
&f_{H+\bar H}(n_f+1,\mu^2)\\
&\quad \equiv f_{n_f+1}(n_f+1,\mu^2) + f_{\overline{n_f+1}}(n_f+1,\mu^2)\\
&\quad = \tilde A_{Hq}^{\rm PS}\Big(n_f, \frac{\mu^2}{m^2}\Big) \otimes \Sigma(n_f,\mu^2)\\
&\quad +\tilde A_{Hg}^{\rm S}\Big(n_f, \frac{\mu^2}{m^2}\Big) \otimes G(n_f,\mu^2)\,. \qquad (2.38)
\end{aligned}
$$

Comparing the above expression with (2.27) we observe that the first term in (2.27) has no counter part in (2.38). This is because we have no bare heavy-quark density unless one assumes that there already exists an intrinsic heavy-quark component of the proton wave function. The singlet combination of the quark densities becomes

$$
\begin{aligned}
\Sigma(n_f+1,\mu^2) &= \sum_{k=1}^{n_f+1}\Big[f_k(n_f+1,\mu^2) + f_{\bar k}(n_f+1,\mu^2)\Big]\\
&= \Bigg[A_{qq,H}^{\rm NS}\Big(n_f, \frac{\mu^2}{m^2}\Big) + n_f \tilde A_{qq,H}^{\rm PS}\Big(n_f, \frac{\mu^2}{m^2}\Big)\\
&+\tilde A_{Hq}^{\rm PS}\Big(n_f, \frac{\mu^2}{m^2}\Big)\Bigg] \otimes \Sigma(n_f,\mu^2) \qquad (2.39)\\
&+\Bigg[n_f \tilde A_{qg,H}^{\rm S}\Big(n_f, \frac{\mu^2}{m^2}\Big) + \tilde A_{Hg}^{\rm S}\Big(n_f, \frac{\mu}{m^2}\Big)\Bigg] \otimes G(n_f,\mu^2)\,.
\end{aligned}
$$

The non-singlet combination $\Delta_k(n_f+1)$ is defined in an analogous way as in (2.3) and it reads for $k = 1, \ldots, n_f+1$

$$
\begin{aligned}
\Delta_k(n_f+1,\mu^2) &= f_k(n_f+1,\mu^2) + f_{\bar k}(n_f+1,\mu^2)\\
&\quad -\frac{1}{n_f+1}\Sigma(n_f+1,\mu^2)\,. \qquad (2.40)
\end{aligned}
$$

Finally the gluon density for n_f+1 light flavours is

$$
\begin{aligned}
G(n_f+1,\mu^2) &= A_{gq,H}^{\rm S}(n_f,\mu^2) \otimes \Sigma(n_f,\mu^2)\\
&\quad +A_{gg,H}^{S}(n_f,\mu^2) \otimes G(n_f,\mu^2)\,. \qquad (2.41)
\end{aligned}
$$

The old as well as the new parton densities have to satisfy the momentum sum rule

$$
\int_0^1 dx\, x\Big[\Sigma(n_f,x,\mu^2) + G(n_f,x,\mu^2)\Big] = 1\,, \quad (2.42)
$$

for any n_f. This implies that the OME's A_{Hk}, $A_{kl,H}$ have to satisfy two relations

$$
\begin{aligned}
&\int_0^1 dx\, x\Bigg[A_{qq,H}^{\rm NS}\Big(n_f, x, \frac{\mu^2}{m^2}\Big) + n_f \tilde A_{qq,H}^{\rm PS}\Big(n_f, x, \frac{\mu^2}{m^2}\Big)\\
&\quad +\tilde A_{Hq}^{\rm PS}\Big(n_f, x, \frac{\mu^2}{m^2}\Big) + A_{gq,H}^{\rm S}\Big(n_f, x, \frac{\mu^2}{m^2}\Big)\Bigg] = 1\,, \qquad (2.43)
\end{aligned}
$$

and

$$\int_0^1 dx\, x\Bigg[n_f \tilde{A}^{\rm S}_{qg,H}\Big(n_f, x, \frac{\mu^2}{m^2}\Big) + \tilde{A}^{\rm S}_{Hg}\Big(n_f, x, \frac{\mu^2}{m^2}\Big) + A^{\rm S}_{gg,H}\Big(n_f, x, \frac{\mu^2}{m^2}\Big)\Bigg] = 1\,, \tag{2.44}$$

which can be checked up to second order using the results in Appendix B.

The OME's A_{Hk} and $A_{kl,H}$ satisfy the following RGE's

$$\begin{aligned} D\tilde{A}^{\rm PS}_{Hq} = {} & \Big(\gamma^{\rm NS}_{qq} + n_f\tilde{\gamma}^{\rm PS}_{qq}\Big)\otimes\tilde{A}^{\rm PS}_{Hq} + \gamma^{\rm S}_{gq}\otimes\tilde{A}^{\rm S}_{Hg} \\ & -(\gamma^{\rm NS}_{HH} + \tilde{\gamma}^{\rm PS}_{HH})\otimes\tilde{A}^{\rm PS}_{Hq} - \tilde{\gamma}^{\rm S}_{Hg}\otimes A^{\rm S}_{gq,H} \\ & -\tilde{\gamma}^{\rm PS}_{Hq}\otimes\Big(A^{\rm NS}_{qq,H} + n_f\tilde{A}^{\rm PS}_{qq,H}\Big)\,, \end{aligned} \tag{2.45}$$

$$\begin{aligned} D\tilde{A}^{\rm S}_{Hg} = {} & \gamma^{\rm S}_{gg}\otimes\tilde{A}^{\rm S}_{Hg} + n_f\tilde{\gamma}^{\rm S}_{qg}\otimes\tilde{A}^{\rm PS}_{Hq} \\ & -(\gamma^{\rm NS}_{HH} + \tilde{\gamma}^{\rm PS}_{HH})\otimes\tilde{A}^{\rm S}_{Hg} \\ & -\tilde{\gamma}^{\rm S}_{Hg}\otimes A^{\rm S}_{gg,H} - n_f\tilde{\gamma}^{\rm PS}_{Hq}\otimes\tilde{A}^{\rm S}_{qg,H}\,, \end{aligned} \tag{2.46}$$

$$DA^{\rm NS}_{qq,H} = -\gamma^{\rm NS}_{qq,H}\otimes A^{\rm NS}_{qq,H}\,, \tag{2.47}$$

$$\begin{aligned} D\tilde{A}^{\rm PS}_{qq,H} = {} & \gamma^{\rm S}_{gq}\otimes\tilde{A}^{\rm S}_{qg,H} - \Big(\gamma^{\rm NS}_{qq,H} + n_f\tilde{\gamma}^{\rm PS}_{qq,H}\Big)\otimes\tilde{A}^{\rm PS}_{qq,H} \\ & -\tilde{\gamma}^{\rm PS}_{qq,H}\otimes A^{\rm NS}_{qq,H} - \Big(\tilde{\gamma}^{\rm S}_{qg,H} + \tilde{\gamma}^{\rm S}_{qg}\Big)\otimes A^{\rm S}_{gq,H} \\ & -\tilde{\gamma}^{\rm PS}_{qH}\otimes\tilde{A}^{\rm PS}_{Hq}\,, \end{aligned} \tag{2.48}$$

$$\begin{aligned} D\tilde{A}^{\rm S}_{qg,H} = {} & \tilde{\gamma}^{\rm S}_{qg}\otimes\Big(A^{\rm NS}_{qq,H} + n_f\tilde{A}^{\rm PS}_{qq,H}\Big) + \gamma^{\rm S}_{gg}\otimes\tilde{A}^{\rm S}_{qg,H} \\ & -\Big(\gamma^{\rm NS}_{qq,H} + n_f\tilde{\gamma}^{\rm PS}_{qq,H} + \gamma^{\rm NS}_{qq} + n_f\tilde{\gamma}^{\rm PS}_{qq}\Big)\otimes\tilde{A}^{\rm S}_{qg,H} \\ & -\Big(\tilde{\gamma}^{\rm S}_{qg,H} + \tilde{\gamma}^{\rm S}_{qg}\Big)\otimes A^{\rm S}_{gg,H} - \tilde{\gamma}^{\rm PS}_{qH}\otimes\tilde{A}^{\rm S}_{Hg}\,, \end{aligned} \tag{2.49}$$

$$\begin{aligned} DA^{\rm S}_{gq,H} = {} & \Big(\gamma^{\rm NS}_{qq} + n_f\tilde{\gamma}^{\rm PS}_{qq}\Big)\otimes A^{\rm S}_{gq,H} + \gamma^{\rm S}_{gq}\otimes A^{\rm S}_{gg,H} \\ & -\Big(\gamma^{\rm S}_{gq,H} + \gamma^{\rm S}_{gq}\Big)\otimes\Big(A^{\rm NS}_{qq,H} + n_f\tilde{A}^{\rm PS}_{qq,H}\Big) \\ & -\Big(\gamma^{\rm S}_{gg,H} + \gamma^{\rm S}_{gg}\Big)\otimes A^{\rm S}_{gq,H} - \gamma^{\rm S}_{gH}\otimes\tilde{A}^{\rm PS}_{Hq}\,, \end{aligned} \tag{2.50}$$

and

$$\begin{aligned} DA^{\rm S}_{gg,H} = {} & n_f\tilde{\gamma}^{\rm S}_{qg}\otimes A^{\rm S}_{gq,H} - \gamma^{\rm S}_{gg,H}\otimes A^{\rm S}_{gg,H} \\ & -n_f\Big(\gamma^{\rm S}_{gq,H} + \gamma^{\rm S}_{gq}\Big)\otimes\tilde{A}^{\rm S}_{qg,H} - \gamma^{\rm S}_{gH}\otimes\tilde{A}^{\rm S}_{Hg}\,. \end{aligned} \tag{2.51}$$

The above RGE's are much more complicated than those written for A_{kl} in (2.12), (2.13). This is due to the fact already mentioned below (2.36) that μ represents the operator-renormalization scale as well as the mass-factorization scale. In (2.12), (2.13) it only stands for the operator-renormalization scale. The anomalous dimensions coming from operator renormalization carry a minus sign whereas those associated with mass factorization have a plus sign in front of them. This difference in sign can be traced back to (2.14) where it was stated that the residues of the ultraviolet divergences are just the opposite of the ones corresponding to the collinear divergences. Furthermore one has to bear in mind that the residues of the ultraviolet and collinear divergences are equal to the anomalous dimensions coming from operator renormalization and mass factorization respectively. In (2.45)–(2.51) the anomalous dimensions γ_{kl} have a plus sign on account of the collinear divergences occurring in A_{kl}, where the partons indicated by k, l are massless. However the anomalous dimensions γ_{HH}, γ_{Hl}, γ_{lH} and $\gamma_{kl,H}$ carry a minus sign because the mass of the heavy quark m prevents these OME's from being collinearly divergent so that we only have to deal with ultraviolet singularities.

Using the above equations and (2.15)–(2.17) one can derive the RGE's for the new parton densities appearing in $F_i^{\rm VFNS}$ (2.26). For $k = 1, \ldots, n_f + 1$, including the heavy-quark flavour, the RGE reads

$$\begin{aligned} & D\,\Big[f_k(n_f+1,\mu^2) + f_{\bar{k}}(n_f+1,\mu^2)\Big] \\ & = -\gamma^{\rm NS}_{qq}(n_f+1)\otimes\Big[f_k(n_f+1,\mu^2) + f_{\bar{k}}(n_f+1,\mu^2)\Big] \\ & -\tilde{\gamma}^{\rm PS}_{qq}(n_f+1)\otimes\Sigma(n_f+1,\mu^2) \\ & -\tilde{\gamma}^{\rm S}_{qg}(n_f+1)\otimes G(n_f+1,\mu^2)\,. \end{aligned} \tag{2.52}$$

The non-singlet combination of the quark densities satisfies the RGE

$$\begin{aligned} & D\Delta_k(n_f+1,\mu^2) \\ & \quad = -\gamma^{\rm NS}_{qq}(n_f+1)\otimes\Delta_k(n_f+1,\mu^2)\,. \end{aligned} \tag{2.53}$$

The singlet combination of the quark densities satisfies the RGE

$$\begin{aligned} D\Sigma(n_f+1,\mu^2) = {} & -\gamma^{\rm S}_{qq}(n_f+1)\otimes\Sigma(n_f+1,\mu^2) \\ & -\gamma^{\rm S}_{qg}(n_f+1)\otimes G(n_f+1,\mu^2)\,, \end{aligned} \tag{2.54}$$

and the gluon density is given by

$$\begin{aligned} DG(n_f+1,\mu^2) = {} & -\gamma^{\rm S}_{gq}(n_f+1)\otimes\Sigma(n_f+1,\mu^2) \\ & -\gamma^{\rm S}_{gg}(n_f+1)\otimes G(n_f+1,\mu^2)\,. \end{aligned} \tag{2.55}$$

In the above equations we have used the identities

$$\gamma_{ij}(n_f) + \gamma_{ij,H}(n_f) = \gamma_{ij}(n_f+1)\,, \tag{2.56}$$

$$\begin{aligned} \gamma^{\rm NS}_{HH}(n_f+1) &= \gamma^{\rm NS}_{qq}(n_f+1)\,; \\ \tilde{\gamma}^{\rm PS}_{HH}(n_f+1) &= \tilde{\gamma}^{\rm PS}_{qq}(n_f+1)\,, \end{aligned} \tag{2.57}$$

$$\tilde{\gamma}^{\rm PS}_{qH}(n_f+1) = \tilde{\gamma}^{\rm PS}_{Hq}(n_f+1) = \tilde{\gamma}^{\rm PS}_{qq}(n_f+1)\,, \tag{2.58}$$

$$\begin{aligned} \gamma^{\rm S}_{gH}(n_f+1) &= \gamma^{\rm S}_{gq}(n_f+1)\,; \\ \tilde{\gamma}^{\rm S}_{Hg}(n_f+1) &= \tilde{\gamma}^{\rm S}_{qg}(n_f+1)\,, \end{aligned} \tag{2.59}$$

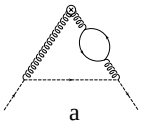

Fig. 3. Two-loop contribution to the OME $A^{\rm S}_{qq,H}$. The *dashed* and *solid lines* represent the light quark q and the heavy quark H respectively

because the anomalous dimensions do not depend on the mass m of the heavy-quark H. A comparison of the above RGE's with those presented for the light-parton densities in (2.15)–(2.17) reveals that they are exactly the same in spite of the fact that there is no counterpart of the bare heavy-quark density in the derivation of (2.52)–(2.55).

All perturbative quantities which appear in this section are now available up to $O(\alpha_s^2)$. This holds for the anomalous dimensions γ_{kl} [16], the massless-parton coefficient functions $\mathcal{C}_{i,k}$ [17] and the heavy-quark coefficient functions $L_{i,k}$, $H_{i,k}$ [4]. The OME's $\tilde{A}^{\rm PS}_{Hq}$, $\tilde{A}^{\rm S}_{Hg}$ and $A^{\rm NS}_{qq,H}$ are computed up to $O(\alpha_s^2)$ and listed in unrenormalized form in Appendix C of [10]. We still require $A^{\rm S}_{qq,H}$ (Fig. 3) and $A^{\rm S}_{gg,H}$ (Fig. 4) which are calculated up to the same order in this paper. Exact expressions for the unrenormalized OME's can be found in Appendix A. Notice that up to second order in α_s both $\tilde{A}^{\rm S}_{qg,H}$ and $\tilde{A}^{\rm PS}_{qq,H}$ are zero. The renormalized (finite) expressions for all these OME's, which we will use in the next section, are presented in Appendix B.

After having found the representation of the heavy-quark density $f_{H+\bar{H}}$ in (2.38) and the RGE in (2.52) which determines its scale evolution we can write down the charm component of the deep-inelastic structure function in the VFNS representation. The latter is given by

$$\begin{aligned} &F_{i,H}^{\rm VFNS}(n_f+1,Q^2) \\ &\quad = e_H^2\Big[f_{H+\bar{H}}(n_f+1,\mu^2)\otimes\mathcal{C}^{\rm NS}_{i,q}\Big(n_f+1,\frac{Q^2}{\mu^2}\Big) \\ &\quad +\Sigma(n_f+1,\mu^2)\otimes\tilde{\mathcal{C}}^{\rm PS}_{i,q}\Big(n_f+1,\frac{Q^2}{\mu^2}\Big) \\ &\quad +G(n_f+1,\mu^2)\otimes\tilde{\mathcal{C}}^{\rm S}_{i,g}\Big(n_f+1,\frac{Q^2}{\mu^2}\Big)\Big]\,. \end{aligned} \tag{2.60}$$

The expression above satisfies $DF_{i,H}^{\rm VFNS}=0$ (see (2.11)), so it is renormalization group invariant, which means that it is scheme independent and becomes a physical quantity. Notice that even though the form of $F_{i,H}^{\rm VFNS}$ is the same as the one presented for intrinsic heavy-quark production, their origins are completely different. In the latter case expression (2.60) is not derived from perturbation theory and therefore there does not exist any relation like (2.38) between the heavy-quark density and the light-parton densities.

Furthermore we want to emphasize that the VFNS approach presented above is only valid for totally inclusive quantities like structure functions since the logarithmic terms $\ln^i(Q^2/m^2)\ln^j(\mu^2/m^2)$ only appear in the asymptotic form of the heavy-quark coefficient functions in this

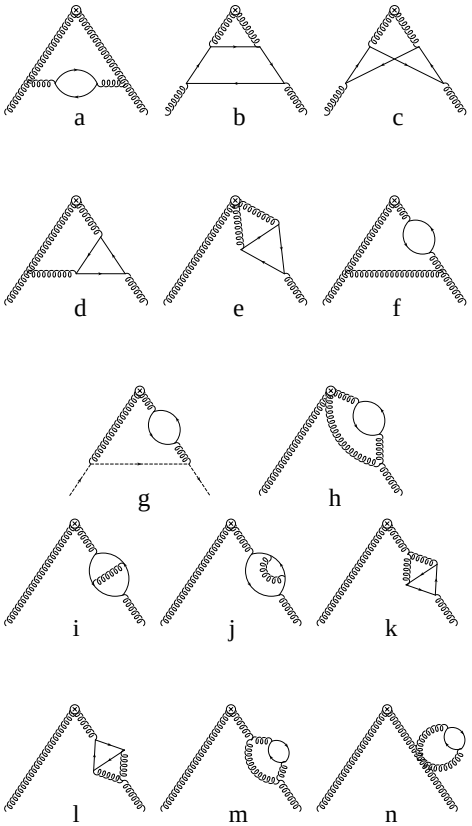

Fig. 4. Two-loop graphs contributing to the OME $A^{\rm S}_{gg,H}$. The *dashed* and *solid lines* represent the Faddeev-Popov ghost and the heavy quark H respectively. The graph with the external Faddeev-Popov ghost (Fig. 4g) has to be included if the sum over the gluon polarization states involves the contributions from unphysical polarizations

case. Hence expression (2.60) is just an alternative description for FOPT when the production of the heavy quarks occurs far above threshold where $Q^2 \gg m^2$. The only difference between the FOPT and the VFNS descriptions is that the large logarithms have been resummed in the latter approach so that one gets an improved expression with respect to normal perturbation theory in the large Q^2-region. These specific large logarithms do not show up in the perturbation series for differential distributions, which depend on a different set of scales. In this case, as has been mentioned in the introduction, one can only distinguish between intrinsic and extrinsic heavy-quark production.

Finally we want to comment about the work in [9] where one has proposed the idea of the VFNS approach. In particular we want to make some remarks about (9) in [9](ACOT) which is similar to our equation (2.60). Using the notations in the latter reference this equation reads

$$\begin{aligned} \sum_\lambda W^\lambda_{BN} = f_N^Q\otimes\sum_\lambda\omega^{\lambda(0)}_{BQ} - f_N^g\otimes f_g^{Q(1)}\otimes\sum_\lambda\omega^{\lambda(0)}_{BQ} \\ +f_N^g\otimes\sum_\lambda\omega^{\lambda(1)}_{Bg}\,, \end{aligned} \tag{2.61}$$

where we have summed over all helicities of the virtual photon denoted by λ. Further we have corrected a mis-

print because $f_g^{Q(0)}$ in (9) should read $f_g^{Q(1)}$. To translate (2.61) into our language we have to make the following replacements

$$B \to \gamma^*\,; \quad Q \to H\,; \quad \sum_\lambda W_{BN}^\lambda \to F_{i,H}^{\rm ACOT}\,, \quad (2.62)$$

$$\sum_\lambda \omega_{BQ}^{\lambda(0)} \to e_H^2\; \mathcal{C}_{i,q}^{\rm NS,(0)} = e_H^2 \delta(1-z)\,;$$
$$\sum_\lambda \omega_{Bg}^{\lambda(1)} \to e_H^2 H_{i,g}^{\rm S,(1)}\,, \quad (2.63)$$

$$f_g^{Q(1)} \to \tilde{A}_{Hg}^{\rm S,(1)}\,, \quad (2.64)$$

and

$$f_N^Q \to f_{H+\bar{H}}\,; \quad f_N^g \to G\,. \quad (2.65)$$

Hence (2.61) can be written in our notation as

$$F_{i,H}^{\rm ACOT} = e_H^2\Big[f_{H+\bar{H}} \otimes \mathcal{C}_{i,q}^{\rm NS,(0)} + G \otimes \tilde{\mathcal{C}}_{i,g}^{\rm S,(1)}\Big] \quad (2.66)$$
$$+e_H^2\,\Big[G \otimes \{H_{i,g}^{\rm S,(1)} - \tilde{\mathcal{C}}_{i,g}^{\rm S,(1)} - \tilde{A}_{Hg}^{\rm S,(1)} \otimes \mathcal{C}_{i,q}^{\rm NS,(0)}\}\Big]\,.$$

Comparing this expression with ours in (2.60) we notice the following differences. First (2.61) and therefore (2.66) in [9] was only derived in lowest order (LO), whereas (2.60) is valid in all orders of perturbation theory. Second (2.61) and (2.66) are not valid in next-to-leading order (NLO) but this can be repaired by replacing $\mathcal{C}_{i,q}^{\rm NS,(0)}$ by $\mathcal{C}_{i,q}^{\rm NS,(0)} + (\alpha_s/4\pi)\,\mathcal{C}_{i,q}^{\rm NS,(1)}$ in (2.66). However the most important difference is that the last term between the square brackets in (2.66) has no counter part in our expression (2.60). This is because we took the limit $Q^2 \to \infty$ and dropped all terms proportional to $(m^2/Q^2)^l$ in the asymptotic heavy-quark coefficient functions. Hence $H_{i,g}^{\rm S,(1)}$ is replaced by $H_{i,g}^{\rm asymp,S,(1)}$ (2.35) so that the last part in (2.66) vanishes. However the exact expressions for $H_{i,g}^{\rm S,(1)}$, $\tilde{\mathcal{C}}_{i,g}^{\rm S,(1)}$ and $\tilde{A}_{Hg}^{\rm S,(1)}$ can be found in the literature (see [4,17] and [10]). Expanding the latter in powers of m^2/Q^2 we obtain

$$H_{i,g}^{\rm S,(1)} - \tilde{\mathcal{C}}_{i,g}^{\rm S,(1)} - \tilde{A}_{Hg}^{\rm S,(1)} \otimes \mathcal{C}_{i,q}^{\rm NS,(0)}$$
$$= \alpha_s(\mu^2) \sum_{l=1}^{\infty} \Big(\frac{m^2}{Q^2}\Big)^l \Big[a_i^{(l)} \ln\Big(\frac{Q^2}{m^2}\Big) + b_i^{(l)}\Big]\,. \quad (2.67)$$

When $Q^2 \to \infty$, (2.67) vanishes as was already expected from the arguments above. The motivation for the above expression, included in [9], was to get a better stability of $F_{i,H}^{\rm VFNS}$ in the threshold region with respect to variations in the factorization scale. However we have dropped these type of contributions as shown in (2.67) in our representation for $F_{i,H}^{\rm VFNS}$ (2.60). A possible generalization of formula (2.66) is given by

$$F_{i,H}^{\rm ACOT}(x,Q^2,m^2) = F_{i,H}^{\rm VFNS}(x,Q^2) + F_{i,H}^{\rm exact}(x,Q^2,m^2)$$
$$-F_{i,H}^{\rm asymp}(x,Q^2,m^2), \quad (2.68)$$

where $F_{i,H}^{\rm VFNS}$, $F_{i,H}^{\rm exact}$ and $F_{i,H}^{\rm asymp}$ are given in (2.60), (2.29) and (2.30). Up to $O(\alpha_s)$, $F_{i,H}^{\rm VFNS}$ and $F_{i,H}^{\rm exact} - F_{i,H}^{\rm asymp}$ correspond with the first and the last parts of (2.66) respectively (for the last part see also (2.67)). Further in (2.66) the term $G \otimes\ H_{i,g}^{\rm S,(1)}$ stands for the lowest order contribution to $F_{i,H}^{\rm exact}$ whereas in the same order $F_{i,H}^{\rm asymp}$ is represented by $G \otimes \{\tilde{\mathcal{C}}_{i,g}^{\rm S,(1)} + \tilde{A}_{Hg}^{\rm S,(1)} \otimes \mathcal{C}_{i,q}^{\rm NS,(0)}\}$. The main idea behind (2.68) is that far above threshold $F_{i,H}^{\rm ACOT}$ is given by $F_{i,H}^{\rm VFNS}$ which requires the cancelation between $F_{i,H}^{\rm exact}$ and $F_{i,H}^{\rm asymp}$. This is happening in LO (see [9]) and in NLO (see the next section). Near threshold $F_{i,H}^{\rm ACOT}$ should be given by $F_{i,H}^{\rm exact}$ so that $F_{i,H}^{\rm VFNS}$ should be cancelled by $F_{i,H}^{\rm asymp}$. According to [9] this happens in LO for charm production but, as we will show in the next section, certainly not in NLO.

3 Validity of FOPT and the VFNS

Now we want to investigate which of the two approaches i.e. FOPT or VFNS, is the most appropriate to describe the total structure functions $F_i(x,Q^2)$ and their charm ($H = c, m = m_c$) components $F_{i,c}(x,Q^2,m_c^2)$ in the different kinematical regimes. In particular we are interested in which region the large logarithms $\ln^i(Q^2/m_c^2)\ln^j(\mu^2/m_c^2)$ dominate the higher order corrections. Further we make a comparison between the parton densities in our VFNS given by (2.37)–(2.41) and the ones in the literature. Finally we study the rate of convergence of the perturbation series near or far away from the charm threshold region which will be different for these two approaches.

Before presenting our results we want to mention that all perturbative quantities like the operator-matrix elements (OME's), heavy-quark coefficient functions and light-parton coefficient functions are presented in the $\overline{\rm MS}$-scheme. Therefore we have to use parton densities parametrized in the same scheme. Furthermore in FOPT the number of light flavours in the running coupling constant and the coefficient functions has to be equal to three ($\Lambda_3 = 232$ MeV (LO); $\Lambda_3 = 248$ MeV (NLO)) whereas in the VFNS this number should be equal to four ($\Lambda_4 = 200$ MeV (LO and NLO)). For the mass of the charm quark and the factorization (renormalization) scale we have chosen $m_c = 1.5$ GeV/c and $\mu^2 = Q^2$ respectively, because this scale is usually adopted for the light-parton components of the structure functions. Notice that in the literature [6,9,12] different scales (containing m_c^2) are chosen for the charm structure function in FOPT. However the NLO results are rather independent of the scale as is shown in [11–13].

First we investigate in which region the large logarithmic terms dominate the heavy quark coefficient functions. To that order we will compute $F_{i,c}^{\rm exact}$ (2.29) and $F_{i,c}^{\rm asymp}$ (2.30) up to NLO. The exact heavy quark coefficient functions occuring in $F_{i,c}^{\rm exact}$, which are given by $L_{i,k}$ and and $H_{i,k}$ ($i = 2, L$ and $k = q, g$), are computed up to $O(\alpha_s^2)$ in [4]. Their asymptotic analogues appearing in $F_{i,c}^{\rm asymp}$ can

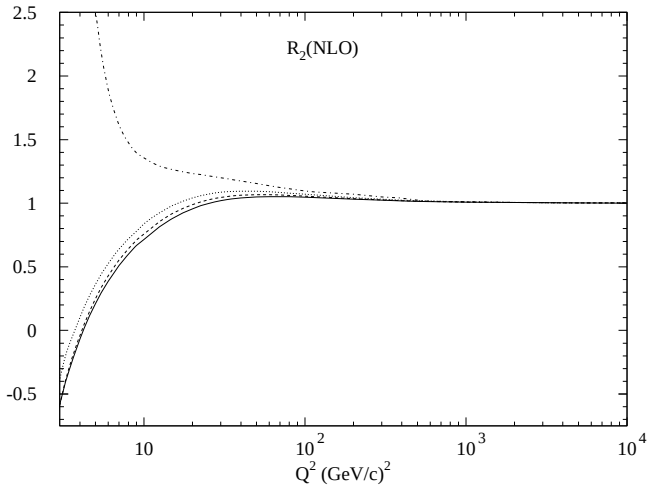

Fig. 5. R_2(NLO) (3.1) plotted as a function of Q^2 at fixed x; $x = 10^{-1}$ (*dashed-dotted line*), $x = 10^{-2}$ (*dotted line*), $x = 10^{-3}$ (*dashed line*) and $x = 10^{-4}$ (*solid line*)

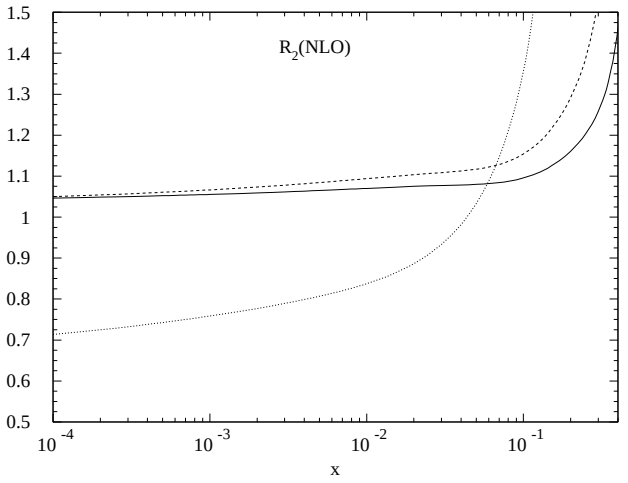

Fig. 6. R_2(NLO) (3.1) plotted as a function of x at fixed Q^2; $Q^2 = 10$ (GeV/c)^2 (*dotted line*), $Q^2 = 50$ (GeV/c)^2 (*dashed line*), $Q^2 = 100$ (GeV/c)^2 (*solid line*)

be found in [10]. The latter are strictly speaking only valid when $Q^2 \gg m_c^2$. In order to determine the x and Q^2 values above which $F_{i,c}^{\rm exact}$ and $F_{i,c}^{\rm asymp}$ coincide we plot the following ratios

$$R_i(x, Q^2, m_c^2) = \frac{F_{i,c}^{\rm asymp}(x, Q^2, m_c^2)}{F_{i,c}^{\rm exact}(x, Q^2, m_c^2)}\,. \qquad (3.1)$$

For these plots we adopt the GRV94HO parton density set [18]. The reason that this set is chosen is because it is obtained from a fit to the deep-inelastic scattering data performed in the spirit of the FOPT approach, which means that the number of active flavours is chosen to be three and the charm component of the structure function is calculated from the photon-gluon fusion process (albeit with a scale depending on m_c^2) and its higher order QCD corrections.

In Fig. 5 we plot R_2(NLO) as a function of Q^2 at some fixed x-values whereas in Fig. 6 similar plots are made for R_2(NLO) as a function of x where Q^2 is kept fixed. From these figures we infer that far above threshold i.e. $s > 1000\, m_c^2$, R_2 gets close to one ($1.1 > R_2 > 0.9$). The above value of s (photon-hadron cm energy squared) corresponds to the kinematical range $x < 10^{-2}$ and $Q^2 > 20$ (GeV/c)^2) explored by the experiments carried out at HERA [6]. The reason that we plot R_i ($i = 2, L$) as a function of x and Q^2 instead of s is that the data are presented for the former variables. The fact that $R_2 \neq 1$ near threshold $s = 4\, m_c^2$, corresponding to large x and small Q^2, can be wholly attributed to threshold terms. The latter, which are mainly due to soft gluon bremsstrahlung, are present in the exact heavy-quark coefficient functions. However they are absent in their asymptotic expressions.

In Figs. 7 and 8 we made similar plots for R_L(NLO). Here the approach to $R_L = 1$ starts at a much larger value of s i.e. $s > 4.10^4\, m_c^2$ which is two orders of magnitude larger than the one found for R_2(NLO). This value corresponds with $x < 10^{-2}$ and $Q^2 > 10^3$ (GeV/c)^2. Here the threshold effects occuring in the exact heavy quark

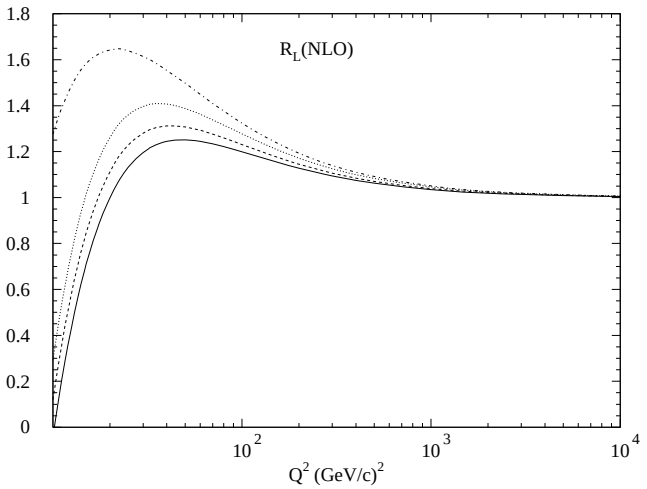

Fig. 7. Same as in Fig. 5 but now for R_L(NLO)

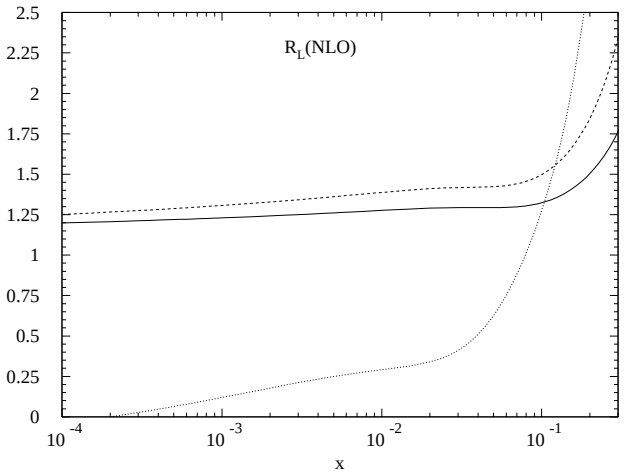

Fig. 8. Same as in Fig. 6 but now for R_L(NLO)

coefficient functions become even more conspicuous than those discovered for R_2(NLO). The reason that threshold effects are dominant at large x and small Q^2 (small s) can be explained when one looks at the convolution

$$\int_x^{z_{\rm th}} \frac{dz}{z} f_k\Big(\frac{x}{z},\mu^2\Big) H_{i,k}\Big(z,\frac{Q^2}{m^2},\frac{m_c^2}{\mu^2}\Big)\,, \tag{3.2}$$

with a similar expression when $H_{i,k}$ is replaced by $L_{i,k}$. Here f_k and $H_{i,k}$,$L_{i,k}$ denote the parton densities and the heavy-quark coefficient functions respectively. The threshold value is given by

$$z_{\rm th} = \frac{Q^2}{Q^2 + 4\ m_c^2} \tag{3.3}$$

in the expression for the structure function (2.29). From the above equations one infers that when x is very large and Q^2 is very small $x \to z_{\rm th}$ so that only threshold terms can contribute to the integral (3.2). We also would like to comment on the phenomenon that the approach to R_i(NLO) $= 1$ is much slower for $i = L$ than for $i = 2$. It originates from the fact that the power of the large logarithms appearing in the heavy-quark coefficient functions in the case of $i = L$ is one unit smaller than that for $i = 2$. This phenomenon was also observed for heavy-flavour production in the Drell-Yan process [19]. It appears that the Q^2 value for which the exact and asymptotic expressions of the physical quantities coincide is smaller when the powers of the large logarithmic terms increase. Notice that the Born contribution to the longitudinal coefficient function does not contain logarithms in the limit $Q^2 \gg m_c^2$ so that it is independent of Q^2 and m_c^2. In this case, as well as in some interference terms in the Drell-Yan process, the convergence to the asymptotic expressions takes place at an extremely large value of Q^2.

We have also studied R_i(LO) in the Born approximation to the charm structure functions in (3.1). Here it turns out that in the threshold region R_i(LO) is closer to one than R_i(NLO) ($i = 2, L$) which means that the threshold effects in the Born approximation are smaller than in the case of the higher order corrections. However above $s = 1000\ m_c^2$ (R_2) or $s = 4.10^4\ m_c^2$ (R_L) we observe that the ratio R_i(NLO) is closer to one than in the case of R_i(LO). In Sect. 5 of [10] we made the same study of R_i in (3.1) but on the level of the heavy-quark coefficient functions themselves. A comparison with the results from [10] reveals that the s value (here the cm energy squared of the photon-parton subprocess) for which the asymptotic and exact heavy-quark coefficient functions coincide is the same as the one obtained for the charm structure functions in (3.1). Hence the convolution with the parton densities in (3.2) hardly affects the x and Q^2 values at which the exact and asymptotic expressions coincide.

Next we discuss the parton densities which emerge from our VFNS approach according to (2.37)–(2.41). The most interesting among them is the charm-quark density which appears in the four-flavour scheme. It is derived from the formula in (2.38) where we choose $n_f = 3$. Up to $O(\alpha_s^2)$ (2.38) becomes equal to

$$\begin{aligned} f_{c+\bar{c}}^{\rm VFNS}(4,x,\mu^2) &\equiv f_4(4,x,\mu^2) + f_{\bar{4}}(4,x,\mu^2) \\ &= \Big(\frac{\alpha_s(\mu^2)}{4\pi}\Big)^2 \int_x^1 \frac{dz}{z} \Sigma\Big(3,\frac{x}{z},\mu^2\Big) \tilde{A}_{cq}^{\rm PS,(2)}\Big(z,\frac{\mu^2}{m_c^2}\Big) \\ &+ \int_x^1 \frac{dz}{z} G\Big(3,\frac{x}{z},\mu^2\Big)\Big[\Big(\frac{\alpha_s(\mu^2)}{4\pi}\Big) \tilde{A}_{cg}^{\rm S,(1)}\Big(z,\frac{\mu^2}{m_c^2}\Big) \\ &+ \Big(\frac{\alpha_s(\mu^2)}{4\pi}\Big)^2 \tilde{A}_{cg}^{\rm S,(2)}\Big(z,\frac{\mu^2}{m_c^2}\Big)\Big]\,, \end{aligned} \tag{3.4}$$

where $\tilde{A}_{cq}^{\rm PS,(2)}$, $\tilde{A}_{cg}^{\rm S,(i)}(i = 1, 2)$ are the OME's presented in (B.1)–(B.3) (with $H = c$) which are renormalized in such a way that α_s in (3.4) depends on four flavours ($\Lambda_4 = 200$ MeV). Further one has to put $n_f = 3$ in the OME's above, which, up to order α_s^2, are independent of the number of flavours. The quantities $\Sigma(3,\mu^2)$ and $G(3,\mu^2)$ represent the singlet combination of parton densities and the gluon density in the three-flavour scheme respectively. Notice that the $O(\alpha_s)$ term was already introduced in (10) of [9]. From the above equation one infers that up to $O(\alpha_s)$ (LO), $f_{c+\bar{c}}^{\rm VFNS}(4,x,m_c^2) = 0$ due to the vanishing of the lowest order OME $\tilde{A}_{cg}^{\rm S,(1)}$ (B.2) at $\mu = m_c$. However since $\tilde{A}_{cq}^{\rm PS,(2)}$ (B.1) and $\tilde{A}_{cg}^{\rm S,(2)}$ (B.3) do not vanish at $\mu = m_c$ we get $f_{c+\bar{c}}^{\rm VFNS}(4,x,m_c^2) \neq 0$ up to $O(\alpha_s^2)$. It will turn out that the difference with the existing parton density sets, which satisfy the condition $f_{c+\bar{c}}(4,x,m_c^2) = 0$, will be very small because, after resummation of the $\ln^i(\mu^2/m_c^2)$-terms via the RGE, the effect shows up in NNLO only. What one does with the non-logarithmic terms is a question of the choice of scheme. To compare with the scale evolution of the existing parton densities we will remove the non-logarithmic terms in (B.1) and (B.3) so that both the charm quark density in (3.4) and the ones in the literature satisfy the condition $f_{c+\bar{c}}(4,x,m_c^2) = 0$. For a comparison we choose the GRV92HO set [20]. The reason is that the GRV92 set contains a charm-quark density which is not present in the GRV94 set [18]. In Fig. 9 we plot the ratio

$$R_{\rm ch} = \frac{f_{c+\bar{c}}^{\rm VFNS}(4,x,\mu^2)}{f_{c+\bar{c}}^{\rm PDF}(4,x,\mu^2)}\,, \tag{3.5}$$

as a function of μ^2 at some fixed x-values. Here $f_{c+\bar{c}}^{\rm VFNS}$ is computed from (3.4) by choosing the parton density set GRV92HO [20] for the determination of $\Sigma(3,\mu^2)$ and $G(3,\mu^2)$ while $f_{c+\bar{c}}^{\rm PDF}$ is the charm-quark density belonging to the same set. For $x < 10^{-2}$ it turns out that $1 > R_{\rm ch} > 0.9$. This is surprising because (3.4) is calculated up to finite order in perturbation theory whereas the GRV density is the NLO solution of the RGE's in which all leading and next-to-leading logarithms are resummed. Hence we should expect a larger difference between the scale evolutions. However from the results in [21,22] we anticipate that this difference is not so dramatic as long as $\mu^2/m_c^2 < 10^3$. Apparently the leading logarithms beyond $O(\alpha_s^2)$, which are neglected in (3.4), but not in the GRV charm quark density, do not play an important role provided μ^2 is not chosen to be too large. We have also made a comparison with other charm quark densities in the literature like the ones from CTEQ [23] and MRS [24] and we found a similar result for the scale evolution. However

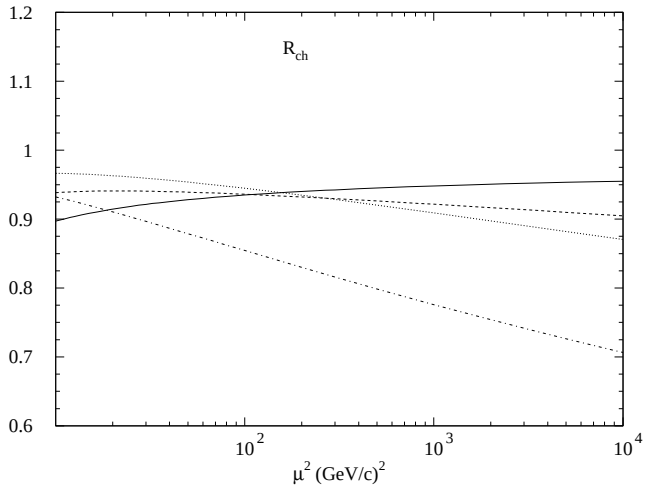

Fig. 9. The ratio $R_{\rm ch} = f_{c+\bar{c}}^{\rm VFNS}/f_{c+\bar{c}}^{\rm PDF}$ (3.5) as a function of μ^2 at fixed x in NLO. The charm densities $f_{c+\bar{c}}^{\rm VFNS}$ and $f_{c+\bar{c}}^{\rm PDF}$ are given by (3.4) and the set GRV92HO [20] respectively; $x = 10^{-1}$ (*dashed-dotted line*), $x = 10^{-2}$ (*dotted line*), $x = 10^{-3}$ (*dashed line*), $x = 10^{-4}$ (*solid line*)

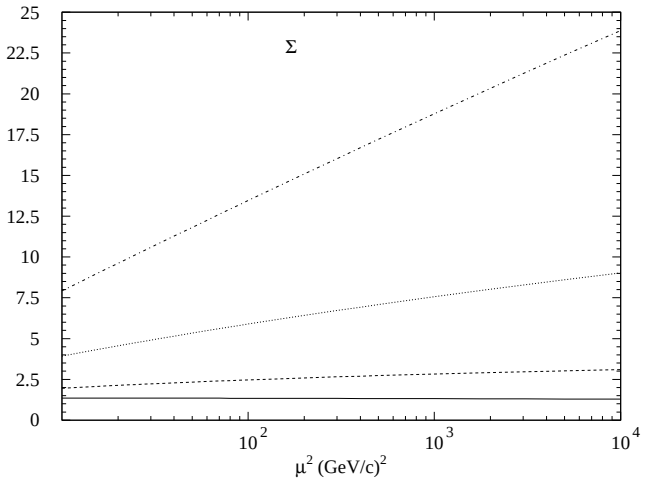

Fig. 10. $\Sigma(3, x, \mu^2)$ and $\Sigma'(4, x, \mu^2)$ (the difference between both singlet combinations of quark densities is unnoticeable in the figure) plotted as functions of μ^2 at fixed x; $x = 10^{-1}$ (*solid line*), $x = 10^{-2}$ (*dashed line*), $x = 10^{-3}$ (*dotted line*), $x = 10^{-4}$ (*dashed-dotted line*)

in the latter sets $R_{\rm ch}$ deviates more from one than shown by [20]. Notice that in [20,23] and [24] all parton densities are presented in a four flavour scheme whereas in (3.4) one should have chosen for $\Sigma(3, \mu^2)$ and $G(3, \mu^2)$ a three flavour scheme. However the differences between the representations for the three and four flavour schemes of the light parton densities (u,d,s) and g are very small as we will show below. The modification for the light-quark densities is given by (2.37). Summing the latter over the three light flavours (u,d and s) one obtains the singlet density corrected up to $O(\alpha_s^2)$ which is given by

$$\Sigma'(4, x, \mu^2) = \int_x^1 \frac{dz}{z} \Sigma\Big(3, \frac{x}{z}, \mu^2\Big) \times \Big[\delta(1-z) + \Big(\frac{\alpha_s(\mu^2)}{4\pi}\Big)^2 A_{qq,c}^{\rm NS,(2)}\Big(z, \frac{\mu^2}{m_c^2}\Big)\Big], \quad (3.6)$$

where $A_{qq,c}^{\rm NS,(2)}$ is given in (B.4) (with $H = c$). Notice that $\Sigma(4, x, \mu^2) = \Sigma'(4, x, \mu^2) + f_{c+\bar{c}}(4, x, \mu^2)$ in (2.39). Up to $O(\alpha_s^2)$ the gluon density in the four-flavour scheme (see (2.41)) is

$$G(4, x, \mu^2) = \Big(\frac{\alpha_s(\mu^2)}{4\pi}\Big)^2 \int_x^1 \frac{dz}{z} \Sigma\Big(3, \frac{x}{z}, \mu^2\Big) A_{gq,c}^{\rm S,(2)}\Big(z, \frac{\mu^2}{m_c^2}\Big) + \int_x^1 \frac{dz}{z} G\Big(3, \frac{x}{z}, \mu^2\Big) \Big[\delta(1-z) + \Big(\frac{\alpha_s(\mu^2)}{4\pi}\Big) A_{gg,c}^{\rm S,(1)}\Big(z, \frac{\mu^2}{m_c^2}\Big) + \Big(\frac{\alpha_s(\mu^2)}{4\pi}\Big)^2 A_{gg,c}^{\rm S,(2)}\Big(z, \frac{\mu^2}{m_c^2}\Big)\Big]. \quad (3.7)$$

The functions $A_{gq,c}^{\rm S,(2)}$ and $A_{gg,c}^{\rm S,(i)}$ $(i = 1, 2)$ are given in (B.5)-(B.7) (with $H = c$). Notice that up to $O(\alpha_s^2)$ the above OME's are independent of the number of internal flavours n_f. In Fig. 10 we show the singlet combinations of parton densities $\Sigma(3, \mu^2)$ and $\Sigma'(4, \mu^2)$ (3.6) and, as the difference between them is $O(\alpha_s^2)$, it is essentially invisible.

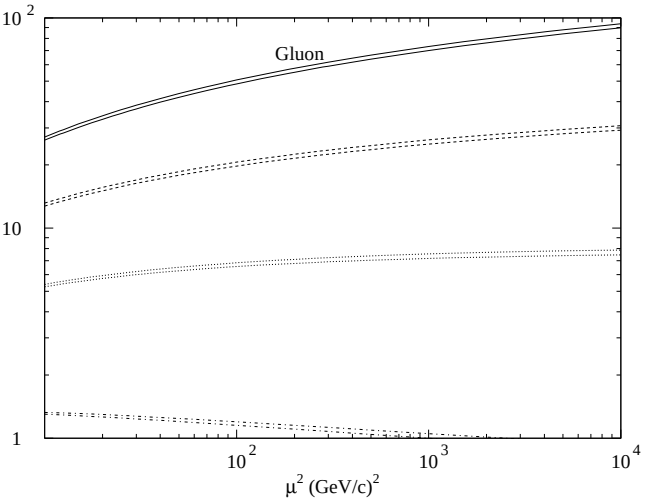

Fig. 11. $G(3, x, \mu^2)$ (*lower lines*) and $G(4, x, \mu^2)$ (*upper lines*) plotted as functions of μ^2 at fixed x; $x = 10^{-1}$ (*dashed-dotted line*), $x = 10^{-2}$ (*dotted line*), $x = 10^{-3}$ (*dashed line*), $x = 10^{-4}$ (*solid line*)

Therefore the error made in choosing $\Sigma(3, \mu^2)$ instead of $\Sigma'(4, \mu^2)$ above the charm threshold is extremely small. In Fig. 11 we make the same study for the gluon density where we compare $G(3, \mu^2)$ with $G(4, \mu^2)$. Here the latter function yields the higher curves. In this case the difference is larger than for the singlet-quark combination (3.6). This is no surprise because for the gluon density the modification already starts on the $O(\alpha_s)$ level (see (3.7)).

Summarizing our findings above we can conclude that for the actual computation of the charm structure function in (2.60), it does not makes much difference when the light-flavour densities computed via (3.4), (3.6) and (3.7) (using fixed order perturbation theory) are replaced by those obtained from the various parton-density sets avail-

able in the literature. To distinguish between the use of (3.4), (3.6), (3.7) and the parton densities in the literature for the computation of (2.60) we denote the corresponding charm structure functions in the subsequent part of this section by $F_{2,c}^{\rm VFNS}$ and $F_{2,c}^{\rm PDF}$, respectively.

Now we want to study the differences between the FOPT and VFNS approaches for the description of the charm structure function $F_{2,c}$. Using the set GRV92HO [20] we present plots in Figs. 12a–e for $F_{2,c}^{\rm exact}$ (2.29) (FOPT) and $F_{2,c}^{\rm VFNS}$ (2.60) which are computed up to NLO. From these figures we infer that at large x and for Q^2-values greater than $Q^2 = 3$ (GeV/c)^2 one hardly sees any difference between both approaches so that threshold effects in $F_{2,c}^{\rm exact}$ are invisible. However at small x ($x < 10^{-2}$) the difference between $F_{2,c}^{\rm exact}$ and $F_{2,c}^{\rm VFNS}$ becomes more conspicuous. It is in this region that data will appear from the HERA collider experiments. Although the difference is not that large at $Q^2 = 3$ (GeV/c)^2 it becomes big for $5 < Q^2 < 10$ (GeV/c)^2 (see Figs. 12b,c). Here $F_{2,c}^{\rm VFNS}$ exceeds $F_{2,c}^{\rm exact}$ by more than 60% with respect to the latter quantity at $x = 10^{-4}$. The difference becomes less when Q^2 increases, e.g. at $Q^2 = 100$ (GeV/c)^2 (Fig. 12e) it is about 25%. This is an indication of the size of resummation effects in this region. Further we have also plotted $F_{2,c}^{\rm asymp}$ (2.30). As expected from Figs. 5,6 this function approaches $F_{2,c}^{\rm exact}$ in the region far above the charm production threshold i.e. $x < 10^{-2}$ and $Q^2 > 20$ (GeV/c)^2. We did not plot $F_{2,c}^{\rm asymp}$ at $Q^2 = 3$ (GeV/c)^2 (Fig. 12a) because here it becomes negative for $x < 0.1$ (threshold region !). From Figs. 12b–e one observes a noticeable difference between $F_{2,c}^{\rm asymp}$ and $F_{2,c}^{\rm VFNS}$. This is because $F_{2,c}^{\rm asymp}$ is computed up to order α_s^2 whereas $F_{2,c}^{\rm VFNS}$ also involves α_s^3 contributions. The latter are due to the convolutions in (2.60) of the order α_s^2 corrected densities in (3.4), (3.6) and (3.7) with the order α_s corrected light-parton coefficient functions. Due to the large logarithms these order α_s^3 contributions are quite appreciable and they survive in the region $3 < Q^2 < 100$ (GeV/c)^2 covered by our plots. The corrections beyond order α_s^2 present in $F_{2,c}^{\rm VFNS}$ can be resummed using the RGE's in (2.52)–(2.55). This procedure has been applied to obtain the parton densities (here GRV92HO) present in $F_{2,c}^{\rm PDF}$. Figs. 12a–e show that $F_{2,c}^{\rm PDF}$ is slightly larger than $F_{2,c}^{\rm VFNS}$ which is not surprising because the parton densities represent the resummation of the large logarithms appearing beyond O(α_s^2).

We also want to comment on the presentation of the charm structure function according to [9] (ACOT) of which the generalization is given in (2.68). In the previous figures we have seen that for $Q^2 > 20$(GeV/c)^2, $F_{i,c}^{\rm exact}$ approaches $F_{i,c}^{\rm asymp}$ so that $F_{i,c}^{\rm ACOT}$ coincides with $F_{i,c}^{\rm VFNS}$. Therefore $F_{i,c}^{\rm ACOT}$ gives a good description of the charm structure function at large Q^2-values. However at small Q^2, $F_{i,c}^{\rm VFNS} \neq F_{i,c}^{\rm asymp}$ (see Figs .12b–e) so that $F_{i,c}^{\rm ACOT}$ is not dominated by $F_{i,c}^{\rm exact}$. Therefore $F_{i,c}^{\rm ACOT}$ (2.68) does not have the correct threshold behaviour exhibited by $F_{i,c}^{\rm exact}$. The inequality between $F_{i,c}^{\rm VFNS}$ and $F_{i,c}^{\rm asymp}$ is due to the large value of $\alpha_s(Q^2)$ and the different ways the corrections beyond $O(\alpha_s)$ have been included in the latter two functions. In our case $F_{i,c}^{\rm asymp}$ is computed up $O(\alpha_s^2)$ whereas $F_{i,c}^{\rm VFNS}$ even contains $O(\alpha_s^3)$ contributions. If $F_{i,c}^{\rm VFNS}$ is replaced by $F_{i,c}^{\rm PDF}$ the above inequality becomes even larger since the latter even includes contributions beyond $O(\alpha_s^3)$. Due to these considerations and the fact that the large logarithms only become relevant far above threshold the expressions for $F_{i,c}^{\rm asymp}$, $F_{i,c}^{\rm VFNS}$ and $F_{i,c}^{\rm PDF}$ have no physical meaning in the region given by large x and low Q^2. Hence they cannot be considered as a good approximation in this region and the charm structure function should only be represented by $F_{i,c}^{\rm exact}$. We have also studied the total structure function $F_2(x, Q^2)$, where the charm component is included. Since this structure function is dominated by the light-parton (u,d,s and g) contributions the differences between the various descriptions is much smaller than those observed for the charm component. At maximum these differences are of the order of 10%, which occurs in the region $5 < Q^2 < 10$ (GeV/c)^2.

To study the stability of the perturbation series for $F_{i,c}$ one can proceed in two different ways. The first one is discussed in [9] and concerns the behaviour of the charm structure function with respect to variations in the factorization scale. It was found that near threshold (large x and small Q^2) $F_{2,c}^{\rm exact}$ shows a better stability than $F_{2,c}^{\rm VFNS}$ under variations of the factorization scale. Far above threshold it turns out that just the opposite happens, so that at large Q^2 it is more preferable to use $F_{2,c}^{\rm VFNS}$ instead of $F_{2,c}^{\rm exact}$ (FOPT). However in the analysis of [9] the NLO corrections from [4] were not taken into account. In [11, 12] and [13] these corrections were included and one could show that far away from threshold $F_{2,c}^{\rm exact}$ is as stable as $F_{2,c}^{\rm VFNS}$ with respect to variations in the factorization scale. The second way to study the stability of the perturbation series is to look at the actual size of the higher order corrections. They have to decrease when the order in α_s increases. To be more specific we study the following quantities

$$K^{(1)} = \frac{F_{2,c}(x,Q^2)({\rm NLO})}{F_{2,c}(x,Q^2)({\rm LO})}\,,$$
$$K^{(2)} = \frac{F_{2,c}(x,Q^2)({\rm NNLO})}{F_{2,c}(x,Q^2)({\rm NLO})}\,. \qquad (3.8)$$

Our criterion is that the perturbation series gets more stable if $K^{(l)} \to 1$ for increasing l where l indicates the order in the perturbation series. Here we want to compare $K^{(1),{\rm exact}}$ (FOPT) with $K^{(l),{\rm VFNS}}$ ($l = 1, 2$), which are derived from $F_{2,c}^{\rm exact}$ (2.29) and $F_{2,c}^{\rm VFNS}$ (2.60), respectively. Both are known in LO and NLO. The structure function $F_{2,c}^{\rm VFNS}$ is also known in NNLO as far as the light-parton coefficient functions (see [17]) are concerned. The NNLO parton densities are not known because the three-loop splitting functions (anomalous dimensions) have not been calculated yet. In virtue of the discussions above we will replace $F_{2,c}^{\rm VFNS}$ by $F_{2,c}^{\rm PDF}$ because this does not appre-

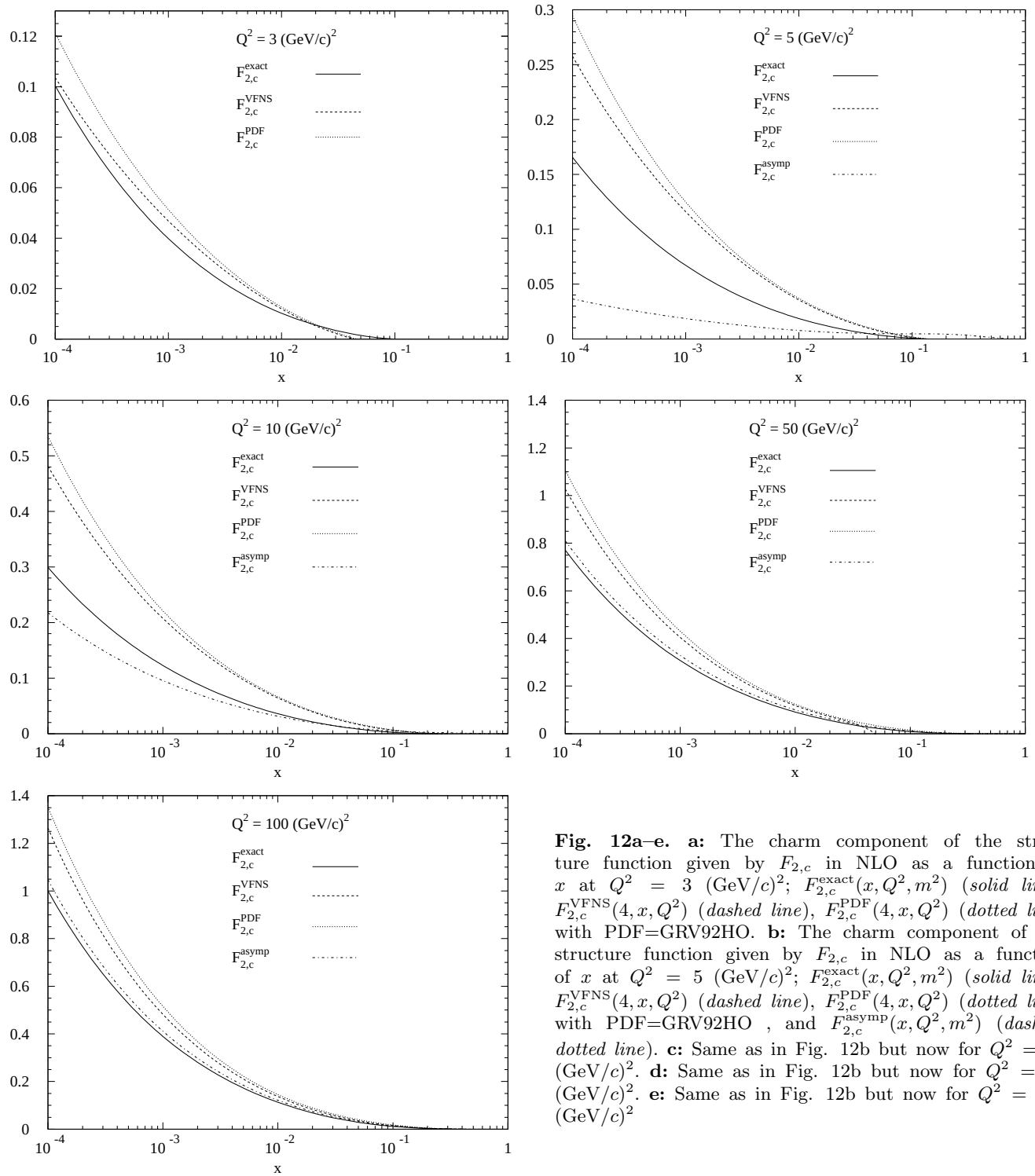

Fig. 12a–e. a: The charm component of the structure function given by $F_{2,c}$ in NLO as a function of x at $Q^2 = 3$ $(\mathrm{GeV}/c)^2$; $F_{2,c}^{\mathrm{exact}}(x, Q^2, m^2)$ (*solid line*), $F_{2,c}^{\mathrm{VFNS}}(4, x, Q^2)$ (*dashed line*), $F_{2,c}^{\mathrm{PDF}}(4, x, Q^2)$ (*dotted line*) with PDF=GRV92HO. **b:** The charm component of the structure function given by $F_{2,c}$ in NLO as a function of x at $Q^2 = 5$ $(\mathrm{GeV}/c)^2$; $F_{2,c}^{\mathrm{exact}}(x, Q^2, m^2)$ (*solid line*), $F_{2,c}^{\mathrm{VFNS}}(4, x, Q^2)$ (*dashed line*), $F_{2,c}^{\mathrm{PDF}}(4, x, Q^2)$ (*dotted line*) with PDF=GRV92HO , and $F_{2,c}^{\mathrm{asymp}}(x, Q^2, m^2)$ (*dashed-dotted line*). **c:** Same as in Fig. 12b but now for $Q^2 = 10$ $(\mathrm{GeV}/c)^2$. **d:** Same as in Fig. 12b but now for $Q^2 = 50$ $(\mathrm{GeV}/c)^2$. **e:** Same as in Fig. 12b but now for $Q^2 = 100$ $(\mathrm{GeV}/c)^2$

ciably change the results. In Figs. 13a–e we plot $K^{(1),\mathrm{exact}}$, $K^{(1),\mathrm{PDF}}$ and $K^{(2),\mathrm{PDF}}$, choosing the set GRV92HO [20]. From these figures we infer that for $Q^2 < 5$ $(\mathrm{GeV}/c)^2$, $K^{(1),\mathrm{exact}}$ is rather close to unity over the whole x-range contrary to $K^{(l),\mathrm{PDF}}$ $(l = 1, 2)$ where the latter deviate from unity in spectacular ways. In the region $5 \leq Q^2 < 10$ $(\mathrm{GeV}/c)^2$ the deviation from unity at small x becomes the same for both K-factors. However at large x $(x > 0.01)$ $K^{(1),\mathrm{exact}}$ is still closer to one than $K^{(1),\mathrm{PDF}}$. This picture changes when $Q^2 \geq 10$ $(\mathrm{GeV}/c)^2$. At large x $(x > 0.01)$, both K-factors equally differ from one but at small x the deviation becomes less for $K^{(l),\mathrm{PDF}}$. When Q^2 increases (see Figs. 13d,e), $K^{(2),\mathrm{PDF}}$ becomes much closer to one than $K^{(1),\mathrm{PDF}}$ even in the large x-region. Here we also no-

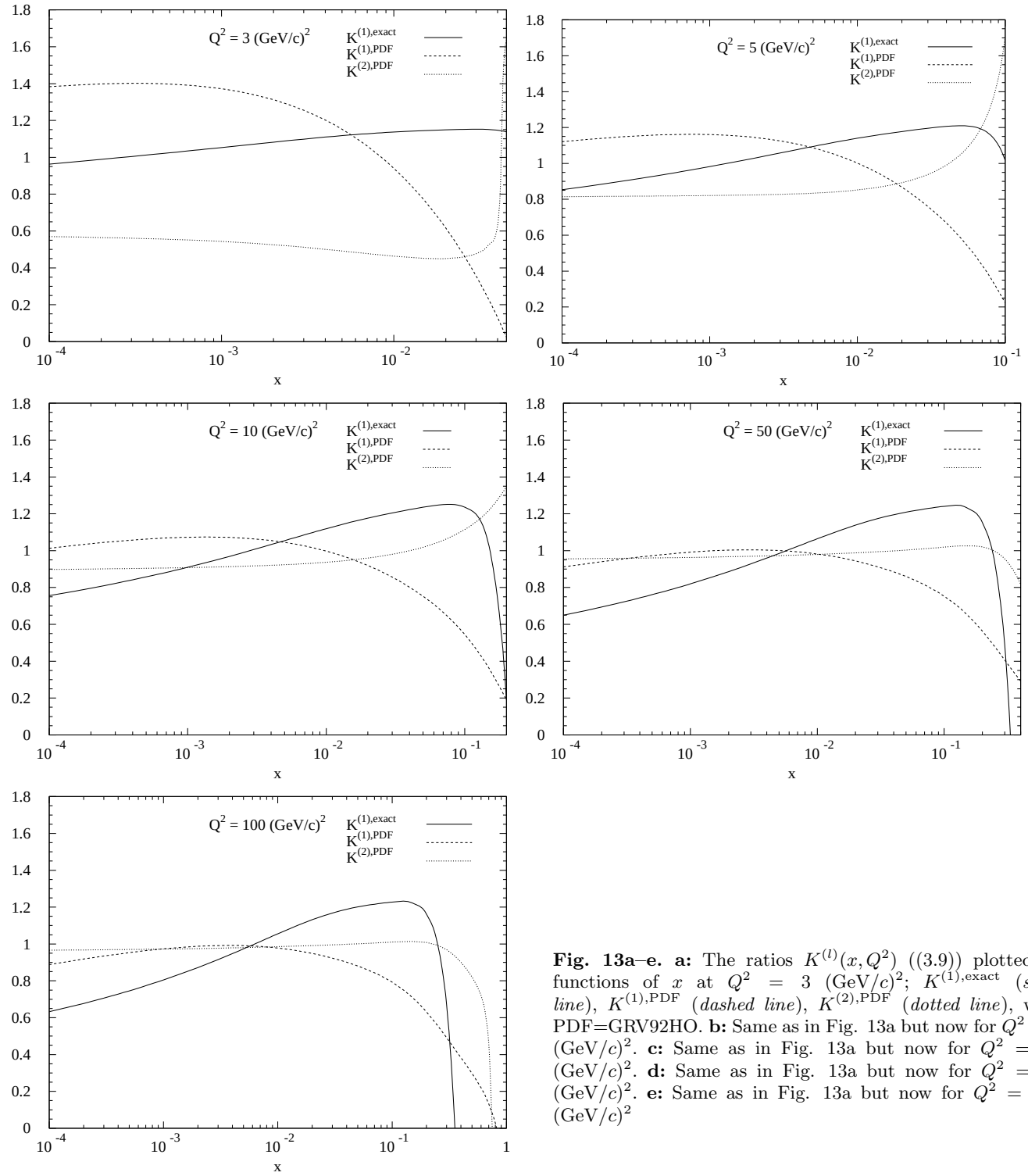

Fig. 13a–e. a: The ratios $K^{(l)}(x, Q^2)$ ((3.9)) plotted as functions of x at $Q^2 = 3$ $(\mathrm{GeV}/c)^2$; $K^{(1),\mathrm{exact}}$ (*solid line*), $K^{(1),\mathrm{PDF}}$ (*dashed line*), $K^{(2),\mathrm{PDF}}$ (*dotted line*), with PDF=GRV92HO. **b:** Same as in Fig. 13a but now for $Q^2 = 5$ $(\mathrm{GeV}/c)^2$. **c:** Same as in Fig. 13a but now for $Q^2 = 10$ $(\mathrm{GeV}/c)^2$. **d:** Same as in Fig. 13a but now for $Q^2 = 50$ $(\mathrm{GeV}/c)^2$. **e:** Same as in Fig. 13a but now for $Q^2 = 100$ $(\mathrm{GeV}/c)^2$

tice a considerable improvement when the NNLO corrections are included. In particular $K^{(2),\mathrm{PDF}}$ is much closer to one than $K^{(1),\mathrm{PDF}}$ at larger Q^2-values, indicating the rapid convergence of the perturbation series in the case of VFNS. If one adopts the convergence of the perturbation series as a criterium to decide about the quality of the two approaches (FOPT versus VFNS) in the various kinematical regimes we conclude that for $Q^2 > 10$ $(\mathrm{GeV}/c)^2$ it is better to use $F_{2,c}^{\mathrm{VFNS}}$ instead of $F_{2,c}^{\mathrm{exact}}$ even when x gets large.

The most important results found in this paper can be summarized as follows. When the charm structure function $F_{2,c}$ is computed in FOPT far above the charm production threshold, given by $x < 0.01$ and $Q^2 >$

20 $(\mathrm{GeV}/c)^2$, the results obtained from the exact ($F_{2,c}^{\mathrm{exact}}$) and the asymptotic heavy-quark coefficient functions ($F_{2,c}^{\mathrm{asymp}}$) are indistinguishable. Hence in this region the large logarithms dominate the perturbation series and they can be resummed after having performed mass factorization on the heavy-quark coefficient functions. In this way starting from $F_{2,c}^{\mathrm{asymp}}$ in the three-flavour scheme one can derive an expression for $F_{2,c}^{\mathrm{VFNS}}$ valid in the four-flavour scheme. This procedure imposes a relation between the parton density sets parametrized at three and four flavours, which has to be satisfied in the VFNS approach. In particular the charm quark density has to satisfy the condition $f_c^{VFNS}(x,m_c^2) \neq 0$ ($\overline{\mathrm{MS}}$-scheme) contrary to what is imposed in the literature. In practice this has no serious consequences for the prediction of $F_{2,c}^{\mathrm{VFNS}}$, which is almost equal to $F_{2,c}^{\mathrm{PDF}}$. Further it turns out that $F_{2,c}^{\mathrm{VFNS}} > F_{2,c}^{\mathrm{exact}}$ for all Q^2-values due to higher-order corrections which are included in VFNS. Finally we have shown that for $x < 0.01$ and $Q^2 < 10$ $(\mathrm{GeV}/c)^2$ the convergence of the perturbation series is better for FOPT than for VFNS. When $Q^2 > 10$ $(\mathrm{GeV}/c)^2$ just the opposite happens. Because of this observation and the fact that the large logarithms dominate in FOPT if $x < 0.01$ and $Q^2 > 20$ $(\mathrm{GeV}/c)^2$ we conclude that in this region the best description of the data is provided by VFNS (see (2.60)). For $Q^2 < 20$ $(\mathrm{GeV}/c)^2$ it is much better to use FOPT (see (2.29)) over the whole x-range. This conclusion is somewhat corroborated by the recent data from the H1-collaboration [6] and the older EMC data on charm production recently examined in [25]. The former data, which are in the range $x < 0.01$ and $10 < Q^2 < 100$ $(\mathrm{GeV}/c)^2$, lie above the predictions of FOPT meaning that VFNS gives a better description. On the other hand the similar Q^2- but large x-data obtained by EMC show that in this case the best theoretical description is given by FOPT.

Acknowledgements. W.L. van Neerven enjoyed some discussions about the charm-quark density with A. Vogt. The research of J. Smith and Y. Matiounine was partially supported by the contract NSF 93-09888. J. Smith would like to thank the Alexander von Humbolt Stiftung for an award to allow him to spend his Sabbatical leave at DESY.

Appendix A

In this appendix we present the unrenormalized operator-matrix elements $\hat{A}_{qq,H}^{\mathrm{S},(2)}$, $\hat{A}_{gg,H}^{\mathrm{S},(1)}$ and $\hat{A}_{gg,H}^{\mathrm{S},(2)}$ where $\hat{A}_{kl,H}^{\mathrm{S},(i)}$ denote the coefficients of $(\alpha_s/4\pi)^i$ in the perturbation series of the operator-matrix elements (OME's). The corresponding two-loop Feynman graphs are presented in Fig. 3 and Fig. 4 respectively and the calculation proceeds in the same way as is outlined for the other OME's in [10]. Using n-dimensional regularization for the ultraviolet and collinear divergences the results are given by ($n = 4 + \epsilon$)

$$\hat{A}_{qq,H}^{\mathrm{S},(2)}\Big(\frac{m^2}{\mu^2},\epsilon\Big) = S_\epsilon^2\Big(\frac{m^2}{\mu^2}\Big)^\epsilon C_F T_f \Bigg\{ \frac{1}{\epsilon^2}\left[\frac{64}{3z} - \frac{64}{3} + \frac{32}{3}z\right]$$
$$+\frac{1}{\epsilon}\left[\frac{160}{9z} - \frac{160}{9} + \frac{128}{9}z + \left(\frac{32}{3z} - \frac{32}{3} + \frac{16}{3}z\right)\ln(1-z)\right]$$
$$+\frac{4}{3}\left(\frac{2}{z} - 2 + z\right)\ln^2(1-z) + \frac{8}{9}\left(\frac{10}{z} - 10 + 8z\right)\ln(1-z)$$
$$+\frac{8}{3}\left(\frac{2}{z} - 2 + z\right)\zeta(2) + \frac{1}{27}\left(\frac{448}{z} - 448 + 344z\right)\Bigg\}. \quad \text{(A.1)}$$

Here S_ϵ denotes the spherical factor which is given by

$$S_\epsilon = \exp\left\{\frac{\epsilon}{2}(\gamma_E - \ln 4\pi)\right\}, \quad \text{(A.2)}$$

where γ_E is the Euler constant.

$$\hat{A}_{gg,H}^{\mathrm{S},(1)}\Big(\frac{m^2}{\mu^2},\epsilon\Big) = S_\epsilon\Big(\frac{m^2}{\mu^2}\Big)^{\frac{\epsilon}{2}}\left[\frac{1}{\epsilon}T_f\left(\frac{8}{3}\delta(1-z)\right)\right], \quad \text{(A.3)}$$

$$\hat{A}_{gg,H}^{\mathrm{S},(2)}\Big(\frac{m^2}{\mu^2},\epsilon\Big) = S_\epsilon^2\Big(\frac{m^2}{\mu^2}\Big)^\epsilon$$
$$\times\Bigg[\frac{1}{\epsilon^2}\Bigg\{C_F T_f\left[32(1+z)\ln z + \frac{64}{3z} + 16 - 16z - \frac{64}{3}z^2\right]$$
$$+C_A T_f\left[\frac{32}{3}\left(\frac{1}{1-z}\right)_+ + \frac{32}{3z} - \frac{64}{3} + \frac{32}{3}z - \frac{32}{3}z^2\right]\Bigg\}$$
$$+\frac{1}{\epsilon}\Bigg\{C_F T_f\left[8(1+z)\ln^2 z + (24+40z)\ln z - \frac{16}{3z} + 64\right.$$
$$\left.-32z - \frac{80}{3}z^2 + 4\delta(1-z)\right]$$
$$+C_A T_f\left[\frac{16}{3}(1+z)\ln z + \frac{80}{9}\left(\frac{1}{1-z}\right)_+ + \frac{184}{9z} - \frac{232}{9}\right.$$
$$\left.+\frac{152}{9}z - \frac{184}{9}z^2 + \frac{16}{3}\delta(1-z)\right]\Bigg\} + a_{gg,H}^{(2)}(z)\Bigg],$$
$$+\sum_{f=H}^{t} S_\epsilon^2\Big(\frac{m_f^2}{\mu^2}\Big)^{\epsilon/2}\Big(\frac{m^2}{\mu^2}\Big)^{\epsilon/2}$$
$$\times\left[\frac{1}{\epsilon^2}T_f^2\left\{\frac{64}{9}\Big(1 + \frac{\epsilon^2}{4}\zeta(2)\Big)\delta(1-z)\right\}\right], \quad \text{(A.4)}$$

with

$$a_{gg,H}^{(2)}(z) = C_F T_f\Bigg\{\frac{4}{3}(1+z)\ln^3 z + (6+10z)\ln^2 z$$
$$+(32+48z)\ln z + 8(1+z)\zeta(2)\ln z$$
$$+\left(\frac{16}{3z} + 4 - 4z - \frac{16}{3}z^2\right)\zeta(2) - \frac{8}{z} + 80 - 48z - 24z^2$$
$$\left.-15\delta(1-z)\right\}$$

$$+C_A T_f \Bigg\{ \frac{4}{3}(1+z)\ln^2 z + \frac{1}{9}(52+88z)\ln z - \frac{4}{3}z\ln(1-z)$$
$$+\frac{8}{3}\left[\left(\frac{1}{1-z}\right)_+ + \frac{1}{z} - 2 + z - z^2\right]\zeta(2)$$
$$+\frac{1}{27}\left[224\left(\frac{1}{1-z}\right)_+ + \frac{556}{z} - 628 + 548z - 700z^2\right]$$
$$+\frac{10}{9}\delta(1-z)\Bigg\}. \qquad \text{(A.5)}$$

The last term in (A.4), which is proportional to T_f^2, is due to the one-loop correction to $\hat{A}^{\mathrm{S},(1)}_{gg,H}$ in (A.3). This correction is represented by the heavy quark (f) loop contribution to the gluon self energy where f represents all heavy flavours starting with the quark H ($m_H \equiv m$) and ending with the top quark t. The corresponding graph is not shown in Fig. 4. In the next section the renormalization of the OME $\hat{A}^{\mathrm{S}}_{gg,H}$ will be chosen in such a way that the heavy quarks with $m_f > m$ decouple from the running coupling constant. This implies that the contributions in the sum of (A.4) with $f > H$ completely vanish in the renormalized OME $\hat{A}^{\mathrm{S}}_{gg,H}$ presented in the next section. However the contribution due to $f = H$ remains in the renormalized expressions like those coming from the n_f light flavours. This renormalization prescription implies that the running coupling constant is presented in the $\overline{\mathrm{MS}}$-scheme and it depends on $n_f + 1$ light flavours including the heavy quark H.

The $1/(1-z)_+$ terms appearing in (A.4) and (A.5) have to be understood as distributions, namely

$$\int_0^1 dz \left(\frac{1}{1-z}\right)_+ f(z) = \int_0^1 dz \frac{1}{1-z}[f(z) - f(1)]\,. \qquad \text{(A.6)}$$

The colour factors in $SU(N)$ are given by

$$C_F = \frac{N^2-1}{2N} \qquad C_A = N \qquad T_f = \frac{1}{2}\,, \qquad \text{(A.7)}$$

with $N = 3$ for QCD.

Appendix B

Here we present the renormalized operator-matrix elements (OME's) corresponding to the unrenormalized expressions given in Appendix C of [10] and in Appendix A of this paper. All OME'S have been renormalized in the $\overline{\mathrm{MS}}$-scheme. In particular the renormalized coupling constant is presented in the above scheme for $n_f + 1$ light flavours. Here the heavy quark H is treated on the same footing as the light flavours and it is not decoupled from the running coupling constant in the VFNS approach. The $(\alpha_s/4\pi)^2$ coefficient in the heavy-quark OME $\tilde{A}^{\mathrm{PS}}_{Hq}$ is given by

$$\tilde{A}^{\mathrm{PS},(2)}_{Hq}\left(\frac{m^2}{\mu^2}\right) = C_F T_f \Bigg\{ \Bigg[-8(1+z)\ln z - \frac{16}{3z} - 4 + 4z$$
$$+\frac{16}{3}z^2\Bigg]\ln^2\frac{m^2}{\mu^2} + \Bigg[8(1+z)\ln^2 z - \left(8 + 40z + \frac{64}{3}z^2\right)\ln z$$
$$-\frac{160}{9z} + 16 - 48z + \frac{448}{9}z^2\Bigg]\ln\frac{m^2}{\mu^2} + (1+z)\Bigg[32\mathrm{S}_{1,2}(1-z)$$
$$+16\ln z\mathrm{Li}_2(1-z) - 16\zeta(2)\ln z - \frac{4}{3}\ln^3 z\Bigg] + \left(\frac{32}{3z} + 8\right.$$
$$\left.-8z - \frac{32}{3}z^2\right)\mathrm{Li}_2(1-z) + \left(-\frac{32}{3z} - 8 + 8z + \frac{32}{3}z^2\right)\zeta(2)$$
$$+\left(2 + 10z + \frac{16}{3}z^2\right)\ln^2 z - \left(\frac{56}{3} + \frac{88}{3}z + \frac{448}{9}z^2\right)\ln z$$
$$-\frac{448}{27z} - \frac{4}{3} - \frac{124}{3}z + \frac{1600}{27}z^2\Bigg\}, \qquad \text{(B.1)}$$

The $(\alpha_s/4\pi)$ and the $(\alpha_s/4\pi)^2$ coefficients of the heavy quark OME $\tilde{A}^{\mathrm{S}}_{Hg}$ are

$$\tilde{A}^{\mathrm{S},(1)}_{Hg}\left(\frac{m^2}{\mu^2}\right) = T_f\left[-4(z^2 + (1-z)^2)\ln\frac{m^2}{\mu^2}\right], \qquad \text{(B.2)}$$

and

$$\tilde{A}^{\mathrm{S},(2)}_{Hg}\left(\frac{m^2}{\mu^2}\right) = \Bigg\{ C_F T_f \Big[(8 - 16z + 16z^2)\ln(1-z)$$
$$-(4 - 8z + 16z^2)\ln z - (2 - 8z)\Big]$$
$$+C_A T_f \Bigg[-(8 - 16z + 16z^2)\ln(1-z) - (8 + 32z)\ln z$$
$$-\frac{16}{3z} - 4 - 32z + \frac{124}{3}z^2\Bigg] + T_f^2\left[-\frac{16}{3}(z^2 + (1-z)^2)\right]\Bigg\}$$
$$\times\ln^2\frac{m^2}{\mu^2} + \Bigg\{ C_F T_f \Bigg[(8 - 16z + 16z^2)[2\ln z\ln(1-z)$$
$$-\ln^2(1-z) + 2\zeta(2)] - (4 - 8z + 16z^2)\ln^2 z$$
$$-32z(1-z)\ln(1-z) - (12 - 16z + 32z^2)\ln z - 56$$
$$+116z - 80z^2\Bigg]$$
$$+C_A T_f \Bigg[(16 + 32z + 32z^2)[\mathrm{Li}_2(-z) + \ln z\ln(1+z)]$$
$$+(8 - 16z + 16z^2)\ln^2(1-z) + (8 + 16z)\ln^2 z + 32z\zeta(2)$$
$$+32z(1-z)\ln(1-z) - \left(8 + 64z + \frac{352}{3}z^2\right)\ln z - \frac{160}{9z}$$

$$+16-200z+\frac{1744}{9}z^2\Bigg]\Bigg\}\ln\frac{m^2}{\mu^2}$$
$$+C_FT_f\Bigg\{(1-2z+2z^2)[8\zeta(3)+\frac{4}{3}\ln^3(1-z)$$
$$-8\ln(1-z)\mathrm{Li}_2(1-z)+8\zeta(2)\ln z-4\ln z\ln^2(1-z)$$
$$+\frac{2}{3}\ln^3 z-8\ln z\mathrm{Li}_2(1-z)+8\mathrm{Li}_3(1-z)-24\mathrm{S}_{1,2}(1-z)]$$
$$+z^2\Bigg[-16\zeta(2)\ln z+\frac{4}{3}\ln^3 z+16\ln z\mathrm{Li}_2(1-z)$$
$$+32\mathrm{S}_{1,2}(1-z)\Bigg]-(4+96z-64z^2)\mathrm{Li}_2(1-z)$$
$$-(4-48z+40z^2)\zeta(2)-(8+48z-24z^2)\ln z\ln(1-z)$$
$$+(4+8z-12z^2)\ln^2(1-z)-(1+12z-20z^2)\ln^2 z$$
$$-(52z-48z^2)\ln(1-z)-(16+18z+48z^2)\ln z+26$$
$$-82z+80z^2\Bigg\}$$
$$+C_AT_f\Bigg\{(1-2z+2z^2)[-\frac{4}{3}\ln^3(1-z)$$
$$+8\ln(1-z)\mathrm{Li}_2(1-z)-8\mathrm{Li}_3(1-z)]+(1+2z+2z^2)$$
$$\times[-8\zeta(2)\ln(1+z)-16\ln(1+z)\mathrm{Li}_2(-z)$$
$$-8\ln z\ln^2(1+z)+4\ln^2 z\ln(1+z)+8\ln z\mathrm{Li}_2(-z)$$
$$-8\mathrm{Li}_3(-z)-16\mathrm{S}_{1,2}(-z)]+(16+64z)[2\mathrm{S}_{1,2}(1-z)$$
$$+\ln z\mathrm{Li}_2(1-z)]-\left(\frac{4}{3}+\frac{8}{3}z\right)\ln^3 z$$
$$+(8-32z+16z^2)\zeta(3)$$
$$-(16+64z)\zeta(2)\ln z+(16z+16z^2)[\mathrm{Li}_2(-z)$$
$$+\ln z\ln(1+z)]$$
$$+\left(\frac{32}{3z}+12+64z-\frac{272}{3}z^2\right)\mathrm{Li}_2(1-z)-\left(12+48z\right.$$
$$\left.-\frac{260}{3}z^2+\frac{32}{3z}\right)\zeta(2)-4z^2\ln z\ln(1-z)$$
$$-(2+8z-10z^2)\ln^2(1-z)+\left(2+8z+\frac{46}{3}z^2\right)\ln^2 z$$
$$+(4+16z-16z^2)\ln(1-z)-\left(\frac{56}{3}+\frac{172}{3}z+\frac{1600}{9}z^2\right)$$
$$\times\ln z-\frac{448}{27z}-\frac{4}{3}-\frac{628}{3}z+\frac{6352}{27}z^2\Bigg\}, \tag{B.3}$$

respectively. Now we present the renormalized expressions for the heavy-quark loop contributions to the light-parton OME's denoted by $A_{kl,H}$. The coefficients of the $(\alpha_s/4\pi)^2$ terms in $A_{qq,H}$ and $A_{gq,H}$ are

$$A_{qq,H}^{\mathrm{NS},(2)}\left(\frac{m^2}{\mu^2}\right)=C_FT_f\Bigg\{\Bigg[\frac{8}{3}\left(\frac{1}{1-z}\right)_+-\frac{4}{3}-\frac{4}{3}z$$
$$+2\delta(1-z)\Bigg]\ln^2\frac{m^2}{\mu^2}+\Bigg[\frac{80}{9}\left(\frac{1}{1-z}\right)_++\frac{8}{3}\frac{1+z^2}{1-z}\ln z+\frac{8}{9}$$
$$-\frac{88}{9}z+\delta(1-z)\left(\frac{16}{3}\zeta(2)+\frac{2}{3}\right)\Bigg]\ln\frac{m^2}{\mu^2}$$
$$+\frac{1+z^2}{1-z}\left(\frac{2}{3}\ln^2 z+\frac{20}{9}\ln z\right)$$
$$+\frac{8}{3}(1-z)\ln z+\frac{224}{27}\left(\frac{1}{1-z}\right)_++\frac{44}{27}-\frac{268}{27}z$$
$$+\delta(1-z)\left(-\frac{8}{3}\zeta(3)+\frac{40}{9}\zeta(2)+\frac{73}{18}\right)\Bigg\}, \tag{B.4}$$

and

$$A_{gq,H}^{\mathrm{S},(2)}\left(\frac{m^2}{\mu^2}\right)=C_FT_f\Bigg\{\Bigg[\frac{16}{3z}-\frac{16}{3}+\frac{8}{3}z\Bigg]\ln^2\frac{m^2}{\mu^2}$$
$$+\left[\frac{160}{9z}-\frac{160}{9}+\frac{128}{9}z+(\frac{32}{3z}-\frac{32}{3}+\frac{16}{3}z)\ln(1-z)\right]$$
$$\times\ln\frac{m^2}{\mu^2}+\frac{4}{3}\left(\frac{2}{z}-2+z\right)\ln^2(1-z)$$
$$+\frac{8}{9}\left(\frac{10}{z}-10+8z\right)\ln(1-z)$$
$$+\frac{1}{27}\left(\frac{448}{z}-448+344z\right)\Bigg\}. \tag{B.5}$$

respectively. The coefficients of the $\alpha_s/4\pi$ and $(\alpha_s/4\pi)^2$ terms in $A_{gg,H}$ are

$$A_{gg,H}^{\mathrm{S},(1)}\left(\frac{m^2}{\mu^2}\right)=T_f\left[\frac{4}{3}\delta(1-z)\ln\frac{m^2}{\mu^2}\right], \tag{B.6}$$

and

$$A_{gg,H}^{\mathrm{S},(2)}\left(\frac{m^2}{\mu^2}\right)=\Bigg\{C_FT_f\Bigg[8(1+z)\ln z+\frac{16}{3z}+4-4z$$
$$-\frac{16}{3}z^2\Bigg]+C_AT_f\left[\frac{8}{3}\left(\frac{1}{1-z}\right)_+-\frac{8}{3z}-\frac{16}{3}+\frac{8}{3}z-\frac{8}{3}z^2\right]$$
$$+T_f^2\left[\frac{16}{9}\delta(1-z)\right]\Bigg\}\ln^2\frac{m^2}{\mu^2}+\Bigg\{C_FT_f\Bigg[8(1+z)\ln^2 z$$
$$+(24+40z)\ln z-\frac{16}{3z}+64-32z-\frac{80}{3}z^2+4\delta(1-z)\Bigg]$$
$$+C_AT_f\left[\frac{16}{3}(1+z)\ln z+\frac{80}{9}\left(\frac{1}{1-z}\right)_++\frac{184}{9z}-\frac{232}{9}\right.$$
$$\left.+\frac{152}{9}z-\frac{184}{9}z^2+\frac{16}{3}\delta(1-z)\right]\Bigg\}\ln\frac{m^2}{\mu^2}$$

$$+C_F T_f \left\{ \frac{4}{3}(1+z)\ln^3 z + (6+10z)\ln^2 z + (32+48z)\ln z \right.$$
$$\left. -\frac{8}{z} + 80 - 48z - 24z^2 - 15\delta(1-z) \right\}$$
$$+C_A T_f \left\{ \frac{4}{3}(1+z)\ln^2 z + \frac{1}{9}(52+88z)\ln z - \frac{4}{3}z\ln(1-z) \right.$$
$$+\frac{1}{27}\left[224\left(\frac{1}{1-z}\right)_+ + \frac{556}{z} - 628 + 548z - 700z^2 \right]$$
$$\left. +\frac{10}{9}\delta(1-z) \right\}, \qquad \text{(B.7)}$$

respectively.

The definitions for the polylogarithms $\mathrm{Li}_n(z)$ and the Nielsen functions $\mathrm{S}_{n,p}(z)$, which appear in the above expressions, can be found in [26]. We have checked that the renormalized OME's given above satisfy the sum rules presented in (2.43) and (2.44). This provides us with a strong check on our results in [10] and in this paper.

References

1. S.J. Brodsky, P. Hoyer, A.H. Mueller, W.-K. Tang, Nucl. Phys. **B369** (1992) 519. R. Vogt and S.J. Brodsky, Nucl. Phys. **B438**, (1995) 261
2. E. Witten, Nucl. Phys. **B104** (1976) 445. J. Babcock and D. Sivers, Phys. Rev. **D18** (1978) 2301. M.A. Shifman, A.I. Vainstein and V.J. Zakharov, Nucl. Phys. **B136** (1978) 157. M. Glück and E. Reya, Phys. Lett. **B83** (1979) 98. J.V. Leveille and T. Weiler, Nucl. Phys. **B147** (1979) 147
3. R.K. Ellis and P. Nason, Nucl. Phys. **B312** (1989) 551. J. Smith and W.L. van Neerven, Nucl. Phys. **B374** (1992) 36
4. E. Laenen, S. Riemersma, J. Smith and W.L. van Neerven, Nucl. Phys. **B392** (1993) 162, 229. S. Riemersma, J. Smith and W.L. van Neerven, Phys. Lett. **B347** (1995) 43. B.W. Harris and J. Smith, Nucl. Phys. **B452** (1995) 109
5. S. Aid et al. (H1-collaboration), Nucl. Phys. **B472** (1996) 32
6. C. Adloff et al. (H1-collaboration), Z. Phys. **C72** (1996) 593
7. S. Riemersma, J. Smith and W.L. van Neerven, Phys. Lett. **B282** (1992) 171. S. Frixione et al. Nucl. Phys. **B412**, (1994) 225; **B431**, (1994) 453
8. M. Glück, E. Hoffmann and E. Reya, Z. Phys. **C13** (1982) 119. M. Glück, R.M. Godbole and E. Reya, Z. Phys. **C38** (1988) 441
9. M.A.G. Aivazis, J.C. Collins, F.I. Olness and W.-K. Tung, Phys. Rev. **D50** (1994) 3102
10. M. Buza, Y. Matiounine, J. Smith, R. Migneron and W.L. van Neerven, Nucl. Phys. **B472** (1996) 611
11. M. Glück, E. Reya and M. Stratmann, Nucl. Phys. **B422** (1994) 37
12. A. Vogt, DESY-96-012, hep-ph/9601352
13. F.I. Olness and S.T. Riemersma, Phys. Rev. **D51** (1995) 4746
14. G. Kramer, B. Lampe and H. Spiesberger, Z. Phys. **C72** (1996) 99
15. A.D. Martin, R.G. Roberts, M.G. Ryskin and W.J. Stirling, DTP/96/102, RAL-TR-96-103
16. G. Curci, W. Furmanski and R. Petronzio, Nucl. Phys. **B175** (1980) 27. W. Furmanski and R. Petronzio, Phys. Lett. **B97** (1980) 437; Z. Phys. **C11** (1982) 293
17. E.B. Zijlstra and W.L. van Neerven, Nucl. Phys. **B383** (1992) 525
18. M. Glück, E. Reya and A. Vogt, Z. Phys. **C67** (1995) 433
19. P.J. Rijken and W.L. van Neerven, Phys. Rev. **D52** (1995) 149
20. M. Glück, E. Reya and A. Vogt, Z. Phys. **C53** (1992) 127
21. E.B. Zijlstra and W.L. van Neerven, Nucl. Phys. **B417** (1994) 61
22. J. Blümlein, S. Riemersma, W.L. van Neerven and A. Vogt, Nucl. Phys. **B** (Proc. Suppl.) 51. **51C** (1996) 96. J. Blümlein et al. , DESY 96-199, hep-ph/9609400, To appear in the proceedings of the workshop "Future Physics at HERA", DESY, Hamburg, 1996
23. H.L. Lai et al. (CTEQ-collaboration), Phys. Rev. **D51** (1995) 4763
24. A.D. Martin, R.G. Roberts and W.J. Stirling, DTP/96/44, RAL-TR-96-037, hep-ph/9606345
25. B.W. Harris, J. Smith and R. Vogt, Nucl. Phys. **B461** (1996) 181
26. L. Lewin, "Polylogarithms and Associated Functions", North Holland, Amsterdam, 1983. R. Barbieri, J.A. Mignaco and E. Remiddi, Nuovo Cimento **11A** (1972) 824. A. Devoto and D.W. Duke, Riv. Nuovo. Cimento Vol. 7,N. 6 (1984) 1